From localized to well mixed: How commuter interactions shape disease spread

Aaron Winn ⬥,[*] Adam Konkol, and Eleni Katifori ⬥

Department of Physics and Astronomy, University of Pennsylvania, Philadelphia, Pennsylvania 19104, USA

Interactions between commuting individuals can lead to large-scale spreading of rumors, ideas, or disease, even though the commuters have no net displacement. The emergent dynamics depend crucially on the commuting distribution of a population, that is how the probability to travel to a destination decays with distance from home. Applying this idea to epidemics, we will demonstrate the qualitatively different infection dynamics emerging from populations with different commuting distributions. If the commuting distribution is exponentially localized, then we recover a reaction-diffusion system and observe Fisher waves traveling at a speed proportional to the characteristic commuting distance. If the commuting distribution has a long tail, then no finite-velocity waves can form, but we show that, in some regimes, there is nontrivial spatial dependence that the well-mixed approximation neglects. We discuss how, in all cases, an initial dispersal-dominated regime can allow the disease to go undetected for a finite amount of time before exponential growth takes over. This "offset time" is a quantity of huge importance for epidemic surveillance and yet largely ignored in the literature.

I. INTRODUCTION

The spread of an infectious disease occurs on several different length scales [1–3]. Long-distance disease transmission has been modeled on global air transport networks by utilizing known air travel rates between major cities [4–6]. At smaller scales, disease can spread within a country along daily commuting networks, and spatial correlations in infection patterns can be observed [7–11]. In either case, the fundamental challenge is to determine when a disease will reach a particular location, as quantified by the infection arrival time [12]. The spatial distribution of arrival times depends on the human mobility patterns. On large scales, the arrival time can be estimated by introducing an effective distance related to the frequency of flights between major cities [13]. On smaller scales, the arrival time is largely determined by the geographic separation between locations. Long-distance travel can quickly turn a local outbreak into a global epidemic. However, once an infectious disease has established itself in a city, the small-scale commuter dynamics become the dominant source of new cases [14]. The goal of this paper is to demonstrate how different commuting patterns give rise to different patterns of disease spread.

Early work studying the spatial spread of infectious disease consisted of continuous models in a uniform population treating the contact rate between individuals as nonlocal [15,16]. When the contact distribution is sufficiently localized, a reaction-diffusion system is recovered, and far from the infection's origin, waves are observed [17]. An overview of the early work on spatial epidemic models can be found in Ref. [18]. These early papers thoroughly studied traveling waves and critical behavior of reaction-diffusion systems

[19,20] but neglected important aspects of a realistic epidemic including the spatially discrete nature of case count data, the asymmetry in the contact distribution, the effects of a nonuniform population, and the precise meaning of the contact distribution as it relates to human mobility.

More recent metapopulation modeling has addressed these theoretical issues. In metapopulation modeling, populations are grouped together into patches where compartmental models can be defined. These patches are isolated, except for some coupling between them [21]. One study by Dirk Brockmann [22] connected human mobility patterns in a metapopulation model to the continuous reaction-diffusion systems studied decades ago. There conservation of population in each patch was enforced by imposing detailed balance on the flux of travelers. Our study revisits some of the calculations performed by Brockmann in a model more appropriate for commuter dynamics where local population conservation is inherent and focuses on a surprisingly ignored aspect of infectious spread: the behavior close to the infection origin. The fact that these reaction-diffusion systems fail to account for long-distance air travel suggests that these models are most applicable over length scales where commuter travel dominates. Not only is the behavior close to the origin theoretically interesting in that it deviates from the well-studied waves displayed at long distances, but it is also the most important regime to study if we care to apply the model to real geographic regions. For many cases, we will see that competition between human dispersal and exponential growth in the number of infections gives rise to a characteristic time at which the disease at any particular location is detected.

The paper is structured as follows. First, we revisit the simple assumptions and consequences of the spatially independent SIR model. Next, we introduce a general metapopulation model based on interactions between two traveling individuals. From this, we focus on localized travel and derive

*winna@sas.upenn.edu

our system of reaction-diffusion equations. Features of these equations are studied numerically and analytically. Finally, we test whether these features survive when used with more complicated and realistic metapopulation models on maps.

II. CONSTRUCTING THE MODEL

A. SIR model

Before attempting to write down a space-dependent epidemic model, it is worth reviewing the assumptions that go into the widely used SIR model, originally formulated by Kermack and McKendrick [23]. The results in this section can be found in any review of compartmental models in epidemiology, e.g., Ref. [24]. Individuals capable of contracting a disease are labeled susceptible. Individuals currently sick and capable of infecting others are labeled infected. Individuals no longer sick are granted lifelong immunity and are labeled recovered. The susceptible $S_{tot}(t)$, infected $I_{tot}(t)$, and recovered $R_{tot}(t)$ populations are tracked with time. Here we use the subscript "tot" to refer to the populations in the entire spatial domain, a distinction which will be necessary once we begin dividing our spatial domain into patches. There are only two parameters in the model: the recovery rate γ and the contact rate β. The recovery rate is simply the inverse of the mean infectious period. The contact rate is a product of two quantities: the expected number of close contacts an individual makes per day ("close" in the sense that there is an opportunity for the disease to spread) and the probability that a close contact with an infected individual will infect a susceptible individual. All individuals in the population are treated equally in that the same rate constants are used for each individual. Furthermore, the population of size N_{tot} is assumed to be well mixed such that contact between any two individuals is equiprobable.

In order to write down the model, one only needs to consider the change in infections in a time Δt. The product $(\beta \Delta t)\frac{I_{tot}}{N_{tot}}$ gives the probability that a susceptible individual will be infected in a time Δt. The total number of new infections must then be weighted by the current susceptible population. Additionally, $(\gamma \Delta t)I_{tot}$ individuals recover. One can then obtain the rate equations for the extensive quantities S_{tot}, I_{tot}, and R_{tot}, but it is often more convenient to work with the intensive quantities $s_{tot} \equiv S_{tot}/N_{tot}$, $i_{tot} \equiv I_{tot}/N_{tot}$, and $r_{tot} \equiv R_{tot}/N_{tot}$,

$$\frac{ds_{tot}}{dt} = -\beta s_{tot} i_{tot}, \tag{1a}$$

$$\frac{di_{tot}}{dt} = +\beta s_{tot} i_{tot} - \gamma i_{tot}, \tag{1b}$$

$$\frac{dr_{tot}}{dt} = +\gamma i_{tot}. \tag{1c}$$

We can rescale time to eliminate one of the β, γ rates, leaving only a single dimensionless parameter $R_0 \equiv \beta/\gamma$ governing the infection dynamics. This is the basic reproduction number which can be interpreted as the expected number of people an infected person infects in a completely susceptible population. If $R_0 < 1$, then the disease-free equilibrium is stable, leading to exponential decay of infections. If $R_0 > 1$, then the disease-free equilibrium is unstable, leading to exponential growth in

infections until herd immunity is reached, at which point $i_{tot}(t)$ reaches a peak value i_{max} and begins to fall to zero. Assuming $s_{tot}(0) \approx 1$ and $i_{tot}(0) \ll 1$, the peak in the infection fraction satisfies

$$i_{max} = 1 - \frac{1 + \ln(R_0)}{R_0}. \tag{2}$$

The fraction of individuals who are at any point infected is given by solving the following transcendental equation for $r_{tot}(\infty)$:

$$r_{tot}(\infty) + \frac{\ln[1 - r_{tot}(\infty)]}{R_0} = 0. \tag{3}$$

The signatures i_{max} and $r_{tot}(\infty)$ will even be present in the space-dependent models we will derive later.

One final quantity which will have an important analogy in the space-dependent model is the arrival time $t_{arrival}$, defined as the time at which i_{tot} exceeds some small threshold value i_c. At early times when $s_{tot} \approx 1$, the linearization of (1b) gives

$$i_{tot}(t) \approx i_{tot}(0)e^{(\beta-\gamma)t}. \tag{4}$$

Equating this expression to i_c and solving for t gives

$$t_{arrival} = \frac{1}{(\beta - \gamma)} \ln\left[\frac{i_c}{i_{tot}(0)}\right]. \tag{5}$$

B. Metapopulation epidemic models

Spatial epidemic models were originally formulated for a uniform-density continuous population by Kendall [15]. He argued that the condition for criticality and the final epidemic size are identical to that of the spatially independent model. Later, he showed that by approximating the interactions between susceptible and infected individuals by a term of the form $s\nabla^2 i$, one finds that the disease spreads as a wave with a minimum speed [16], analogous to the result by Fisher [25]. Mollison proved the existence of waves with a minimum speed without having to resort to the diffusion approximation by carefully choosing an exponential form for the contact rates [26]. He also showed that if the contact distribution is at least exponentially localized, then wave solutions can be expected, but otherwise, the infection propagates at an infinite speed [17].

More recent works define epidemic models in metapopulations. Metapopulation epidemic models can further be divided into two categories depending on how human mobility is incorporated [21,27]. In Lagrangian movement models, individuals have a well-defined home patch but may make contact with individuals outside their home patch, spreading disease. The number of infected individuals who reside in a particular location is tracked with time. In Eulerian models, individuals migrate between patches. The number of infected individuals currently occupying a given patch is tracked with time. The terms "Eulerian" and "Lagrangian" parallel their use in fluid dynamics. For Lagrangian models, the dynamics track the people while for Eulerian models, the dynamics track the patch. The predictions made by these two classes of mobility models are not the same [27]. Each of these models possesses advantages and disadvantages. Lagrangian models automatically satisfy the intuitive constraint that the total population of each patch is constant in time, reflecting the cyclic nature

of commuting patterns. Lagrangian models only keep track of human mobility in as much as it is necessary to define nonlocal contact rates. This may seem like a simpler way to capture the propagation of disease without focusing too much on the motion of individuals, but relating the nonlocal contact rates to human mobility is more subtle in the Lagrangian formulation. This has led to some variation in the formulation of Lagrangian models [7,8,10,28].

The Eulerian models do not inherently satisfy population conservation unless detailed balance is assumed [22]. At small geographic scales, this seems like an unnatural assumption since it allows for the possibility of two individuals to swap positions permanently, but it has been found to be a good approximation on the worldwide air-transportation network [29]. The master equation describing human mobility can be easily written down in a Eulerian model. Rvachev and Longini first presented a Eulerian model [4], and later work focused on calculating critical behavior [30] and effective network distances governing the arrival time [12,13]. Some models have combined aspects of these models by taking into account explicit Eulerian movement of individuals while also enforcing that the individuals travel back to a well-defined home, as is typically only done in Lagrangian models [30–33].

C. Lagrangian movement model

Before introducing our commuter model, we present a mathematical introduction to epidemic models incorporating Lagrangian movement of individuals. In (Lagrangian) metapopulation models, we replace each of our differential equations (1a)–(1c) with n_C differential equations, one for each of the n_C patches, which will also be referred to as counties, or counties in the rest of this work. The contact rate β is replaced by a *contact matrix* $\boldsymbol{\beta}$ with elements β_{nk} describing the interaction between susceptible individuals who live at n and infected ones who live at k. In continuous models, $\boldsymbol{\beta}$ is also referred to as the *contact distribution*. A precise physical interpretation of $\boldsymbol{\beta}$ will be made clear in the next section.

The space-dependent rate equations now read:

$$\frac{ds_n}{dt} = -s_n \sum_k \beta_{nk} i_k, \tag{6a}$$

$$\frac{di_n}{dt} = +s_n \sum_k \beta_{nk} i_k - \gamma i_n, \tag{6b}$$

$$\frac{dr_n}{dt} = +\gamma i_n. \tag{6c}$$

The symbol i_n denotes the proportion of infected people at n, $i_n = I_n/N_n$, where I_n is the number of people living at n who are infected and N_n is the total number of people living at n. Similar equations can be found in Ref. [21], for instance.

We will assume that the number of contacts each person makes in a day and the infectiousness of the disease are the same regardless of where the person lives; that is, we can define the space-independent contact rate,

$$\beta \equiv \sum_k \beta_{nk}. \tag{7}$$

Relaxing this assumption would leave us with a space-dependent contact rate β_n that describes how individuals in

different locations either make contact with more or fewer people per day or how the infectiousness of a disease changes at different locations, but for this paper, we will neglect these considerations and instead focus on different contact matrices which satisfy (7).

The system (6) also possesses a disease-free equilibrium when $s_n = 1$, $i_n = 0$, $r_n = 0$ for all n. The stability of the disease-free equilibrium will be determined by the eigenvalues of the Jacobian,

$$J_{nk} \equiv \left. \frac{\partial i_n}{\partial i_k} \right|_{s_n=1} = \beta_{nk} - \gamma \delta_{nk} \tag{8}$$

of the infected compartment. The vector $(1, \ldots, 1)^T$ is always an eigenvector of this linearized system with eigenvalue $\beta - \gamma$, so if $\beta - \gamma > 0$, then the disease-free equilibrium is unstable. The converse is also true: If $\beta - \gamma < 0$, then the disease-free equilibrium is stable. To show this, we need to demonstrate that in this case all eigenvalues of $\mathbf{J}$ have negative real parts. The following argument is adapted from Ref. [34]. Since $-\mathbf{J}$ is a Z matrix (nonpositive off-diagonal entries), $-\mathbf{J}$ has eigenvalues with positive real parts if and only if there exists a $\vec{v} > 0$ such that $-\mathbf{J}\vec{v} > 0$ (in which case $-\mathbf{J}$ is an M matrix). Using $\vec{v} = (1, \ldots, 1)^T$, we have $-\mathbf{J}\vec{v} = -(\beta - \gamma)\vec{v}$, so if $\beta - \gamma < 0$, then the eigenvalues of $\mathbf{J}$ have negative real parts. Thus, we can define $R_0 \equiv \beta/\gamma$, and the condition for stability is identical to that of the spatially independent model.

We can estimate the final size of the epidemic at each location $r_n(\infty)$ by defining $\bar{r}_n \equiv \sum_k \frac{\beta_{nk}}{\beta} r_k$ and noting that (6c) implies $\frac{d\bar{r}_n}{dt} = \frac{1}{R_0} \sum_k \beta_{nk} i_k$. Dividing this expression by Eq. (6a) allows us to solve for $\bar{r}_n(\infty)$:

$$\frac{d\bar{r}_n}{ds_n} = -\frac{1}{R_0 s_n} \Rightarrow \bar{r}_n(\infty) + \frac{\ln[1 - \bar{r}_n(\infty)]}{R_0} = 0. \tag{9}$$

Notice that $\bar{r}_n(\infty)$ satisfies the same equation as $r_{\text{tot}}(\infty)$ and is therefore spatially independent. The solution to the linear equation relating $\bar{r}_n(\infty)$ to $r_k(\infty)$ is to have $r_k(\infty) = \bar{r}_n(\infty) = r_{\text{tot}}(\infty)$. The contact matrix encodes important spatial information, but the final size of the epidemic is still fixed by R_0.

D. Commuter model

The previous subsection establishes the general framework for Lagrangian metapopulation models in terms of the contact matrix $\boldsymbol{\beta}$. Next we will derive a particular form of $\boldsymbol{\beta}$ used to describe commuter dynamics. The method of derivation will be similar to that in Sec. II A, only now we must find ΔI_n, the increase in infections at county n in a time Δt. We imagine that an individual travels to work, makes contact with people from other counties, and then returns home. Recent work by Le Treut *et al.* has demonstrated how a data-driven Lagrangian formalism can predict the spread of COVID-19 [8]. Some theoretical work has focused on identifying emergent length scales characterizing the spread of disease on a network [5,13]. One work by Dirk Brockmann was particularly influential to our study in attempting to connect the travel rates in a Eulerian framework to the diffusion of infection in real space [22]. Our Lagrangian approach follows directly from a Bayesian derivation and considers the most general
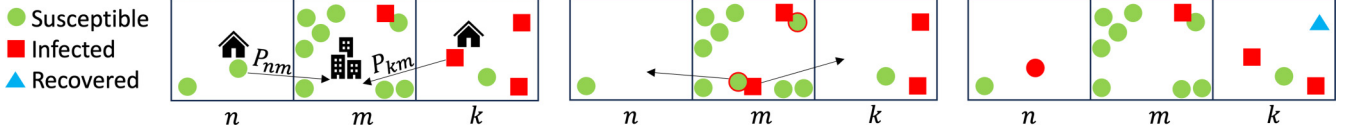
FIG. 1. Commuter dynamics. A susceptible individual from county n and an infected individual from k make contact at m and return home. A green (light gray) circle with a red (dark gray) boundary indicates an infectious contact event.

interactions where both susceptible and infected individuals travel. Many of the results will parallel those derived by Brockmann, but it is important to reassert that the quantities we consider in the Lagrangian formalism are not identical to the related quantities in the Eulerian formalism.

Let P_{nm} denote the fraction of contacts made by the population living at location n that occur at location m, with $\sum_m P_{nm} = 1$. The quantity P_{nn} denotes the fraction of contacts made in the county of residence. Roughly speaking, P_{nm} can be thought of as the probability of an individual who lives at n traveling to m, so we will simply refer to P_{nm} as the *commuting probability*. This probability could depend on the separation of the counties as well as on the populations of any county, but we assume that P_{nm} is independent of disease status. When a person travels from n to m, they will encounter not only individuals who live at m but also individuals who live at other locations k that have traveled to county m. An example interaction between a susceptible and an infected individual is shown in Fig. 1. The probability to make infectious contact at m is equal to the fraction of people currently at m (in the Eulerian sense) who are infected, regardless of where our traveler lives. With this in mind, we can calculate the probability that a worker from n makes infectious contact,

$$\text{Pr(inf. contact|live at } n) = \sum_m \text{Pr(travel to } m|\text{live at } n)$$
$$\times \text{Pr(inf. contact|travel to } m)$$
$$= \sum_m P_{nm} \frac{\sum_k P_{km} I_k}{\sum_k P_{km} N_k}. \qquad (10)$$

This quantity plays the role of I/N in the SIR model. It gives the probability for a particular close contact made by someone living at n to be infectious. We can now easily write down the full *commuter model*:

$$\frac{dS_n}{dt} = -\beta S_n \sum_m P_{nm} \frac{\sum_k P_{km} I_k}{\sum_k P_{km} N_k}, \qquad (11a)$$

$$\frac{dI_n}{dt} = +\beta S_n \sum_m P_{nm} \frac{\sum_k P_{km} I_k}{\sum_k P_{km} N_k} - \gamma I_n, \qquad (11b)$$

$$\frac{dR_n}{dt} = +\gamma I_n. \qquad (11c)$$

In terms of the intensive quantities, the model reads as follows:

$$\frac{ds_n}{dt} = -\beta s_n \sum_m P_{nm} \frac{\sum_k P_{km} N_k i_k}{\sum_k P_{km} N_k}, \qquad (12a)$$

$$\frac{di_n}{dt} = +\beta s_n \sum_m P_{nm} \frac{\sum_k P_{km} N_k i_k}{\sum_k P_{km} N_k} - \gamma i_n, \qquad (12b)$$

$$\frac{dr_n}{dt} = +\gamma i_n. \qquad (12c)$$

All sums are taken over the n_c counties. Similar equations have been derived by other authors [7,10].

We can now identify the contact matrix,

$$\beta_{nk} = \beta \sum_m P_{nm} \frac{P_{km} N_k}{\sum_l P_{lm} N_l}. \qquad (13)$$

Calvetti *et al.* arrived at the same form of the contact matrix by recognizing the ratio in Eq. (13) as the conditional probability of an individual living at county k given that they have traveled to county m [10]. Notice that the contact matrix β_{nk} is not symmetric in a heterogeneous population. However, the matrix $N_n \beta_{nk}$ is precisely the number of close contacts made per time where one individual is from n and one individual is from k; this is necessarily a symmetric matrix. In the special case of a homogeneous population, $P_{lm} = P_{ml}$, so $\beta_{nk} = (\mathbf{P}\mathbf{P}^T)_{nk} = \beta_{kn}$. Here it is particularly clear that we have one factor of $\mathbf{P}$ for the commutes of susceptible individuals and one for the commutes of the infected. We need both of these matrices in order to fully capture the pair interactions between susceptible and infected individuals.

Although we assume β is constant throughout the paper, it is briefly worth mentioning how one could modify the model to account for spatially varying contact rates. Because the contacts occur at the destination m, one would have to make the replacement $\beta \sum_m \to \sum_m \beta_m$. This causes the infection growth rate, $i_{n,\max}$, $r_n(\infty)$, and properties related to the spreading to all have a strong space dependence. Since we are mainly interested in the spatial aspects of commuting patterns, we will avoid the complexity introduced by nonuniform contact rates.

In order to better understand the form of these equations and the relation to Eulerian models, let us see what happens when travel outside of the home county is small. Letting $P_{nm} = \delta_{nm} + \epsilon_{nm}$ and keeping only terms linear in ϵ leads to the following simplification:

$$\beta S_n \sum_m P_{nm} \frac{\sum_k P_{km} I_k}{\sum_k P_{km} N_k}$$
$$\approx \beta S_n \frac{I_n}{N_n} + \beta \frac{S_n}{N_n} \sum_{m \neq n} (N_n P_{nm} + N_m P_{mn}) \left(\frac{I_m}{N_m} - \frac{I_n}{N_n} \right). \qquad (14)$$

This resembles a Eulerian SIR model with symmetric travel flux $\beta(N_n P_{nm} + N_m P_{mn})$ [13]. The first term describes local growth, and the terms in the sum describe movement of the disease. There are two dominant ways the disease can move: A susceptible travels from n and meets an infected at m or an infected travels from m and meets a susceptible at n. The more general form (10) also allows for both the susceptible and the infected to travel, as in Fig. 1, which we will refer to as second-order processes (in $\mathbf{P}$). Interestingly, the second-order

processes can be unimportant in predicting the spread of the infection wave for several choices of **P** but are crucial for understanding the spread in some cases. This simplified form is identical to that used by Le Treut *et al.* [8] who neglect second-order processes.

For numerical simulations, the more general commuter dynamics (10) will always be used. Equation (12) will be solved numerically in Python using the solve_ivp function in the SciPy library with method "RK45."

E. Human mobility theory

While some metapopulation models incorporate known, specific travel rates for particular locations [5,7–10], we are interested to understand the basic principles underlying infection spread so we will take advantage of the research on general human mobility patterns. Traditionally, human mobility was described using gravity models, that is, models which assume that the flux of individuals traveling between two locations is proportional to the populations of the two counties multiplied by some decreasing function of the separation distance (such as a power law, truncated power law, exponential, or Gaussian). In such models, there exists at least one length scale describing how far people travel. See Ref. [35] for a review on models for human mobility. Recently, people have become interested in the radiation model of human mobility that describes an individual's tendency to search for work at the closest location a job is available [36]. This model does not have any inherent travel length scale, only emergent length scales derived from the population distribution. Although the radiation model could be incorporated into (10), the existence of an inherent length scale is going to make it easier to study the general features of our theory, so we will only focus on gravity models in this paper. Thus, we assume the travel probabilities can be cast in the form

$$P_{nm} = \frac{N_m^\zeta G(|\vec{x}_n - \vec{x}_m|)}{\sum_m N_m^\zeta G(|\vec{x}_n - \vec{x}_m|)}, \tag{15}$$

where $\int G(|\vec{x}|)d^d x = 1$. The function G will be referred to as the (homogeneous) *commuting distribution*, since $G(|\vec{x}_m - \vec{x}_n|)$ describes how far people are willing to commute in a homogeneous population. Physically, the sum in the normalization is always taken over a domain containing a finite number of counties, so there is no need to worry about convergence. Still, it will be helpful to think about length scales in the problem that may, in some cases, allow us to take the continuum limit, and in special cases, allow us to derive local transport operators.

Many works find that a truncated power law,

$$G(|\vec{x}|) = \frac{e^{-|\vec{x}|/l}}{(|\vec{x}| + r_0)^p} \bigg/ \int_\Omega \frac{e^{-|\vec{x}|/l}}{(|\vec{x}| + r_0)^p} d^d x, \tag{16}$$

with appropriate choices of p, l, and $r_0 \ll l$ describes human mobility, as summarized in [37]. Note that the special case of a power law can be obtained by setting $l = \infty$, and the special case of an exponential distribution corresponds to setting $p = 0$. When both $p = 0$ and $l = \infty$, the commuting distribution is uniform, so the population is well mixed.

To demonstrate how to perform these calculations, first consider a uniform population on a square grid with lattice constant Δx in d dimensions. The domain will be denoted Ω. Suppose the population changes slowly over a length scale greater than that of Δx. Then, we can take the continuum limit $\Delta x \to 0$ and work in terms of a continuous population density $N_m \to N(\vec{x}_m)d^d x_m$ as well as the probability density function,

$$P_{nm} \to P(\vec{x}_n, \vec{x}_m)d^d x_m = \frac{N(\vec{x}_m)^\zeta G(|\vec{x}_m - \vec{x}_n|)d^d x_m}{\int_\Omega N(\vec{x}_m)^\zeta G(|\vec{x}_m - \vec{x}_n|)d^d x_m}. \tag{17}$$

In many cases, $G(|\vec{x}_m - \vec{x}_n|)$ is presumably localized near $\vec{x}_m = \vec{x}_n$, so one could try to Taylor expand the factor of $N(\vec{x}_m)^\zeta$ around $\vec{x}_n$. However, if $G(|\vec{x}_m - \vec{x}_n|)$ is a power law, then some of the moments of $\vec{x}$ will diverge. Mollison proved that wave solutions exist if and only if the contact distribution falls off faster than exponential at long distances [17]. For our problem, this suggests that we can try to replace our integral expressions with local differential operators (acting on N and i) only if $G(|\vec{x}|)$ falls off faster than exponential. In this case, we can approximate

$$P(\vec{x}_n, \vec{x}_m) \approx \big[1 + \zeta \partial_\mu \ln N(\vec{x}_n)\big(x_m^\mu - x_n^\mu\big)\big]G(|\vec{x}_m - \vec{x}_n|). \tag{18}$$

This is a simpler form to work with, which makes it clear that there is a tendency that increases with ζ to travel toward higher populations. There were multiple approximations which went into putting the population in this simple form. We can summarize these approximations by comparing length scales. Let l denote the characteristic length scale contained in G describing how far people are willing to travel for work, and let L denote the size of the domain,

$$\Delta x \ll l \quad \text{(continuum limit)}, \tag{19}$$

$$x \ll L \quad \text{(neglect boundary effects)}, \tag{20}$$

$$\exists k > 0 \text{ s.t. } \int_\Omega e^{k|\vec{x}|} G(|\vec{x}|)d^d x < \infty \quad \text{(localized)}. \tag{21}$$

Having Δx smaller than other relevant length scales allows us to take the continuum limit. When our model is applied to data, Δx can be interpreted as the county size, and it may not be the smallest length scale, but for studying our theory, there is nothing preventing us from refining the domain until this inequality is satisfied. When L is much larger than other relevant length scales, we can ignore boundary effects allowing us to drop odd moments of x and assert that the even moments are independent of n. Rewriting our integral equations in terms of local operators and moments is valid whenever (21) is satisfied. This technique is only helpful if we can truncate the Taylor series after a few terms, so one might think that l needs to be less than the length scale over which the population changes in order to derive (18), but we will see that the short-wavelength population fluctuations will not change the large-scale infection dynamics.

Localized commuting does not necessarily imply that the infection is confined to a small region of space, especially in small systems where the infection quickly reaches the boundary. To avoid confusion, the term *localized* will be reserved

for commuting distributions satisfying (21), and commuting distributions such as power laws which do not satisfy (21) will be called *delocalized*. Infectious spread which is confined to certain regions of space at a given time will be called *heterogeneous*, and infection growth which is nearly uniform in space will be called *homogeneous*. The term *well mixed* may be applied either to a population with spatially independent contact distribution $G(|\vec{x}|) = 1/L^d$ such that (1) is recovered, or more generally to any contact processes which give rise to nearly homogeneous spreading, even if G is nonconstant. Finally, the term *uniform population* refers to a population with $N_n = $ constant such that $\mathbf{P}$ and $\boldsymbol{\beta}$ are symmetric.

III. CONTINUUM RESULTS

In the next two sections, we study the results of the commuter model. In this section, we will work under approximation (19) and assume the commuting probabilities take the form (17). We will work in terms of the continuous infection density $I(\vec{x}, t)$ and population density $N(\vec{x})$ by making the replacements

$$I_n(t) \to I(\vec{x}_n, t)d^d x_n, \tag{22}$$

$$N_n \to N(\vec{x}_n)d^d x_n, \tag{23}$$

$$i(\vec{x}, t) \equiv \frac{I(\vec{x}, t)}{N(\vec{x})}. \tag{24}$$

Note that, unlike $I(\vec{x}, t)$ and $N(\vec{x})$, $i(\vec{x}, t)$ is unitless. Simulations will always necessarily be performed using the discretized quantities, but when discretized on a square lattice with side length Δx, one can convert to the continuous infection density at the lattice site by dividing by $(\Delta x)^d$; for example, $I(\vec{x}_n, t) = I_n(t)/(\Delta x)^d$. Because the step size falls out of our continuous results, even when the underlying map over which I_n is calculated is not a lattice, the continuum model will give us an estimate for I_n, provided that (19) is satisfied.

Analogously to the contact matrix (13), we can define the contact distribution as follows:

$$\beta(\vec{x}, \vec{z}) = \beta \int_\Omega d^d y \, P(\vec{x}, \vec{y}) \frac{P(\vec{z}, \vec{y})N(\vec{z})}{\int_\Omega d^d w \, P(\vec{w}, \vec{y})N(\vec{w})}, \tag{25}$$

describing interactions between susceptible individuals at $\vec{x}$ and infected individuals at $\vec{z}$. This continuous contact distribution was also obtained in Ref. [10]. Equation (12b) becomes

$$\frac{\partial i(\vec{x}, t)}{\partial t} = s(\vec{x}, t) \int_\Omega d^d z \, \beta(\vec{x}, \vec{z})i(\vec{z}, t) - \gamma i(\vec{x}, t) \tag{26}$$

along with obvious continuum versions for Eqs. (12a) and (12c).

We will encounter moments of the form

$$\langle x^\mu \rangle \equiv \int_\Omega (y^\mu - x^\mu)G(|\vec{y} - \vec{x}|)d^d y, \tag{27}$$

$$\langle x^\mu x^\nu \rangle \equiv \int_\Omega (y^\mu - x^\mu)(y^\nu - x^\nu)G(|\vec{y} - \vec{x}|)d^d y, \tag{28}$$

and so on. When Ω is bounded, all moments will be finite regardless of G, but in an infinite space, all moments will

be finite if and only if (21) is satisfied. It is tempting to set all odd moments to zero and claim that all even moments are independent of home location $\vec{x}$, but this symmetry is only exact in an infinite space or at the origin $\vec{x} = 0$ and will fail considerably near the boundaries. Because no individuals can travel outside of Ω, we must have that the infection flux through the boundary is zero. This amounts to imposing Neumann boundary conditions,

$$\nabla i(\vec{x}, t) \cdot \hat{n} = 0, \quad \vec{x} \in \partial\Omega. \tag{29}$$

A. The diffusion approximation for localized commutes

To begin our analysis of the continuous commuter model, we assume that (21) is satisfied such that we can perform Taylor expansions like those performed to arrive at Eq. (18). Furthermore, we will assume that (20) is satisfied. We will still, in general, consider the problem on a finite domain with (29) satisfied, but (20) will allow us to simplify the moments as follows:

$$\langle x^\mu \rangle \approx 0, \tag{30}$$

$$\langle x^\mu x^\nu \rangle \approx \frac{1}{d} \int |\vec{y} - \vec{x}|^2 G(|\vec{y} - \vec{x}|)d^d y \, \delta^{\mu\nu} \equiv \frac{1}{d}\langle x^2 \rangle \delta^{\mu\nu}. \tag{31}$$

That is, even though our space is finite, we will be using the moments derived from an infinite space where all of the odd moments vanish and the even moments are independent of the home county. Although our commuter model is similar to that of Ref. [10], the analysis in this section most resembles that of earlier papers [16,38]. However, these papers do not account for the effects of a nonuniform population.

To simplify (26), we will take advantage of the localized nature of $G(|\vec{x} - \vec{y}|)$ and perform a series of Taylor expansions up to second order in derivatives of N and i. The details are shown in Appendix A, but the resulting equation is

$$\frac{\partial i}{\partial t} = (\beta s - \gamma)i + \frac{\beta\langle x^2 \rangle}{d}s[\nabla^2 i + \nabla \ln N \cdot \nabla i]. \tag{32}$$

The only mention of our original commuting probability shows up in $\langle x^2 \rangle$, and the parameter ζ falls out completely. Similarly, the second-order contact processes (where both the susceptible and infected travel) only show up in higher-order terms in the Taylor expansion, so we could have derived the same PDE using the simplified form of the contact distribution (14).

The equations resemble a reaction-diffusion system with drift. This is made most explicit by re-expressing the differential equation in terms of I,

$$\frac{\partial I}{\partial t} = \beta s I + s\nabla \cdot (D\nabla I - \vec{v}I) - \gamma I. \tag{33}$$

Here the diffusion coefficient and drift velocity are given by

$$D = \frac{\beta\langle x^2 \rangle}{d} \tag{34}$$

and

$$\vec{v} = \frac{\beta\langle x^2 \rangle}{d}\nabla \ln N, \tag{35}$$

respectively. The infection wave drifts toward higher populations, not because there are more people commuting to work in these places (that would be captured with ζ), but simply because there are more people there capable of spreading infection. Although early modeling papers recognized the relevance of reaction-diffusion equations for the spread of infectious disease [16,18], it is rarely pointed out that a nonuniform population can lead to a drift term. In fact, the only paper to highlight this fact was that of Brockmann [22], who was working in the Eulerian formalism. The fact that the growth rate and the diffusion coefficient both scale with the same rate constant β is an interesting feature which is absent from the Eulerian models and, to our knowledge, seemingly ignored in the mathematical literature.

The diffusion coefficient for the susceptible and infected populations is the same since both arise from the same contact processes, so no Turing patterns can be observed, unlike some models which assume two different diffusion coefficients for the susceptible and infected populations [21,39].

Although the nonlinear PDE (33) cannot be solved analytically, we can study the behavior when almost everybody is susceptible by setting $s = 1$:

$$\frac{\partial I}{\partial t} = (\beta - \gamma)I + \nabla \cdot (D\nabla I - \vec{v}I). \quad (36)$$

We will focus on cases where there is initially some small number of people I_0 infected at the origin:

$$I(\vec{x}, 0) = I_0 \delta^d(\vec{x}). \quad (37)$$

Note that if we integrate (36) over Ω and apply the Neumann boundary conditions, then we will recover the solution $I_{\text{tot}} = I_0 e^{(\beta - \gamma)t}$, the same exponential growth predicted by the spatially independent model. The infection density will immediately spread out and grow. There are two quantities which we will use to characterize this spreading process: the arrival time and the offset time. Although our analysis will be done in the continuum limit in terms of the infection density, these definitions can easily be modified for use with the discrete quantity I_n, so they can be calculated using real county-level data. The *arrival time* t_{arrival} at location $\vec{x}$ is the time it takes for $I(\vec{x}, t)$ to exceed a critical value for the first time: $I(\vec{x}, t_{\text{arrival}}) \geqslant I_c$. The *offset time* t_O is the smallest time which satisfies $I(0, t) \geqslant I_c$ and $\dot{I}(0, t) > 0$. It is useful to think of I_c as the infection density needed to detect the presence of the disease. Then the arrival time $t_{\text{arrival}}(\vec{x})$ indicates how the disease is spreading at early times. The first location for the disease to be detected will typically be near the origin. The offset time is often equivalent to the arrival time at the origin except we also have to check that the infection density is increasing, since we could have $I(0, 0) > I_c$, but $\dot{I}(0, 0) < 0$. Note that the condition $R_0 > 1$ enforces that the total number of infected individuals in the population I_{tot} increases at early times, but it does not enforce that the infection density $I(0, t)$ at the origin must increase. It may be that the recovery rate exceeds the local contact rate initially because people are allowed to make contact with others outside their county, and the disease spreads there. In fact, we will see that for our choice of initial condition, the infection density at the origin $I(0, t)$ will initially decrease for a time $\frac{d}{2}(\beta - \gamma)^{-1}$ before increasing. At early times, the infection spreads out in space

before any one location experiences an outbreak. The offset time is a novel metric for determining how long it will take for the first outbreak to occur. Understanding t_O will reveal an interesting competition between the growth and diffusion processes in our model.

1. Solutions in an infinite domain

We begin our analysis by solving (36) on $\Omega = \mathbb{R}^d$ with boundary condition (29) and initial condition (37). The solution for this case is just the well-known solution to the problem of diffusion with growth

$$I(\vec{x}, t) = I_0 \frac{\exp -\frac{(\vec{x} - \vec{v}t)^2}{4Dt}}{(4\pi Dt)^{d/2}} e^{(\beta - \gamma)t}. \quad (38)$$

This exactly solves (36) when $\vec{v}(\vec{x})$ is constant, but for a slowly varying population, $\vec{v}(\vec{x})$ is also slowly varying, so we can approximate the solution by simply replacing $\vec{v} \to \vec{v}(\vec{x})$. Figure 2(a) shows that the numerical solution to (12b) agrees with (38) at early times while Fig. 2(b) shows that the foot of the wave nearly matches the diffusion solution at all times. At long distances, there is some deviation from the diffusion solution due to the higher-order derivative terms we dropped. For all simulations in this section, an exponential commuting distribution was used. At early times, the infection diffuses from the source. At later times, Fisher waves with height $i_n \approx i_{\text{max}}$ [as given by (2)] can be observed traveling at constant speed; equality holds when N is constant.

To understand why the linearized equations predict the wave front of the nonlinear system, it is worth reviewing some results for pulled waves [40–42]. A pulled wave is a traveling front which is driven by activation at the leading edge, where the dynamics are that of the system linearized around the unstable equilibrium. This is in contrast to a pushed wave which requires activation in the interior part of the front where the full nonlinear dynamics are important. Only for pulled waves it is true that the wave speed of the nonlinear system can be determined by studying the linear system. The infection waves considered in our paper are an example of pulled waves because the infection growth rate $(\beta s_n - \gamma)$ is maximized for $s_n = 1$, so the dynamics are indeed dominated by the behavior at the leading edge where i_n is small. As with all pulled waves, whenever the initial conditions decay in space faster than an exponential, the infection front will converge to a wavelike solution traveling at the Fisher wave velocity with corrections which decay in time [40,43]. For the simple initial condition (37), we can demonstrate this convergence explicitly by calculating the arrival time at different locations.

To calculate the arrival time, we equate (38) to I_c. There is no analytic form for $t_{\text{arrival}}(\vec{x})$, but it is easy enough to solve for $\vec{x}(t_{\text{arrival}})$:

$$\vec{x}(t_{\text{arrival}}) = \vec{v}t_{\text{arrival}}$$
$$\pm \vec{c}t_{\text{arrival}} \sqrt{1 - \frac{\ln\left((4\pi Dt_{\text{arrival}})^{d/2} \frac{I_c}{I_0}\right)}{(\beta - \gamma)t_{\text{arrival}}}}, \quad (39)$$

where $\vec{c} = c\hat{r}$ and

$$c = \sqrt{4D(\beta - \gamma)} = \gamma \sqrt{\frac{4R_0(R_0 - 1)\langle x^2 \rangle}{d}} \quad (40)$$
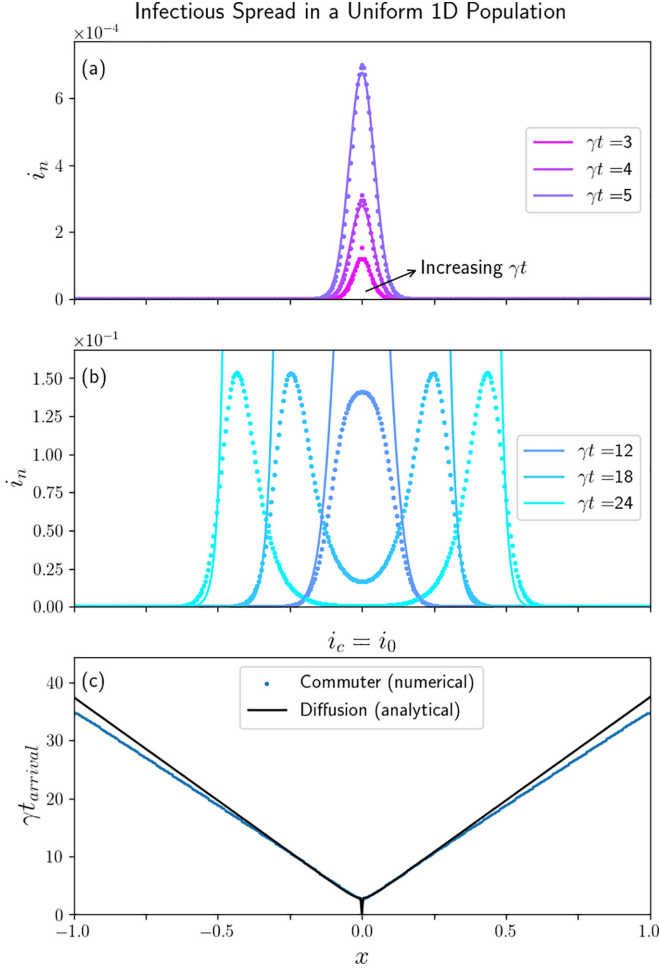
FIG. 2. Infection waves traveling in $d = 1$ from an initial infection at $x = 0$ in a uniform population $N_n = $ constant. In (a) and (b), the fraction of people infected at each location i_n is shown for different times represented by different colors. The points are numerical solutions to Eq. (12b) with $G(|x|) \sim e^{-|x|/l}$, and the solid lines are analytical solutions to (38) multiplied by dx. Parameters used were $dx = 0.005$, $\sqrt{\langle x^2 \rangle} = \sqrt{2l^2} = 0.01$, $i_0 = 10^{-4}$, and $R_0 = 2$. (a) At early times, $s \approx 1$, so our analytical result (38) agrees with the numerical result. (b) For later times, the two solutions disagree, but (38) still captures the propagation of the wave front. (c) The smallest time that solves $i_n(t_{\text{arrival}}) \geqslant i_c$ is displayed for each location.

is the Fisher wave speed [25]. The factor I_c/I_0 will appear throughout our analysis, so it is worth highlighting the fact that this quantity has units of density since I_c is a critical density, whereas I_0 is the initial total infected population. At small times, the expression in the square root may be imaginary, indicating that the disease has yet to be detected anywhere. At late times, the expression in the square root approaches 1, so in a uniform population, the infection front travels at a speed $\vec{v} + \vec{c}$ far from the source. Figure 2(c) shows the arrival time predicted by the commuter model and by the diffusion approximation. The diffusion approximation correctly predicts the offset time, and nearly predicts the speed. Corrections to the speed can be obtained by keeping higher-order derivatives. The fact that the arrival time is linear in x, and the slope is independent of our choice of i_c is a robust property of pulled waves.

When the population distribution is an exponential, the drift velocity is constant. This special case is shown in Fig. 3. When plotted in terms of I_n, the infection drifts toward higher populations, reflecting the fact that there are more people capable of getting infected in more populated regions. When plotted in terms of i_n, the infection drifts toward lower populations, suggesting that a susceptible in a small town is initially at a higher risk of being infected than an individual in a city. However, even in this example with a highly nonuniform population, these drift effects are small, and the shape of the arrival time curves are similar regardless of whether we consider a critical infection count I_c or a critical infection fraction i_c. For this simulation, several values of ζ were chosen with no noticeable differences in the results, consistent with the fact that the ζ corrections show up at fourth order in our Taylor expansion.

In addition to the drift velocity, there is an additional place at which N can enter the calculations even in a constant population. Note that the arrival time in (39) satisfies $I(x, t_{\text{arrival}}) = I_c$, and we used the initial condition $I(x, 0) = I_0\delta(x)$. However, it may make sense for one or both of these conditions to be written in terms of i. If both the arrival condition and the initial condition are given in terms of i, then the factors of N are eliminated. However, suppose one person is initially infected, but the infection is detected at a location when the fraction of cases exceeds a critical value $i(x, t) = i_c$. Then the time offset will have an additional $\ln N$ dependence, reflecting the fact that it takes longer for a disease to be detected in a larger population.

So far, we have only considered long-wavelength population fluctuations. However, there is an opposite limit that is even simpler. When the population changes on the length scale of Δx, we empirically find that we can replace $N(\vec{x})$ with its average value and use the analytic results for the constant population case. See Fig. 4 for an example. This tells us that we can ignore the fact that the population of each county is different if we work in terms of $i(\vec{x}, t)$ and focus only on large-scale population gradients.

Notice in these figures that the numerically calculated arrival time near the origin is greater than zero, indicating that there is some finite time before the infection is detected anywhere. At distances smaller than $\sim\sqrt{\langle x^2 \rangle}$, the analytical arrival time predicted by diffusion appears to be zero, a consequence of the highly localized initial conditions, but this is not a good indicator an outbreak is actually occurring close to the origin. It is clear from looking at these plots that there is a characteristic gap in the arrival time at the origin. We will quantify this gap by finding the offset time. For simplicity, we will focus on the constant population case where $\vec{v} = 0$, so the first outbreak will occur at the origin. As a reminder, by outbreak, we mean two things: First, the infection density must exceed the critical value for detection $I(0, t) \geqslant I_c$, and second, the case counts must be increasing $\dot{I}(0, t) > 0$. The offset time t_O is the smallest time which satisfies both of these conditions. If $R_0 \leqslant 1$, then we can never satisfy the second condition because the infection density at the origin decreases monotonically, so t_O does not exist. If $R_0 > 1$, then the infection initially spreads out causing the infection density to decrease at the origin from its initially infinite value, but at later times exponential growth in the total number of cases
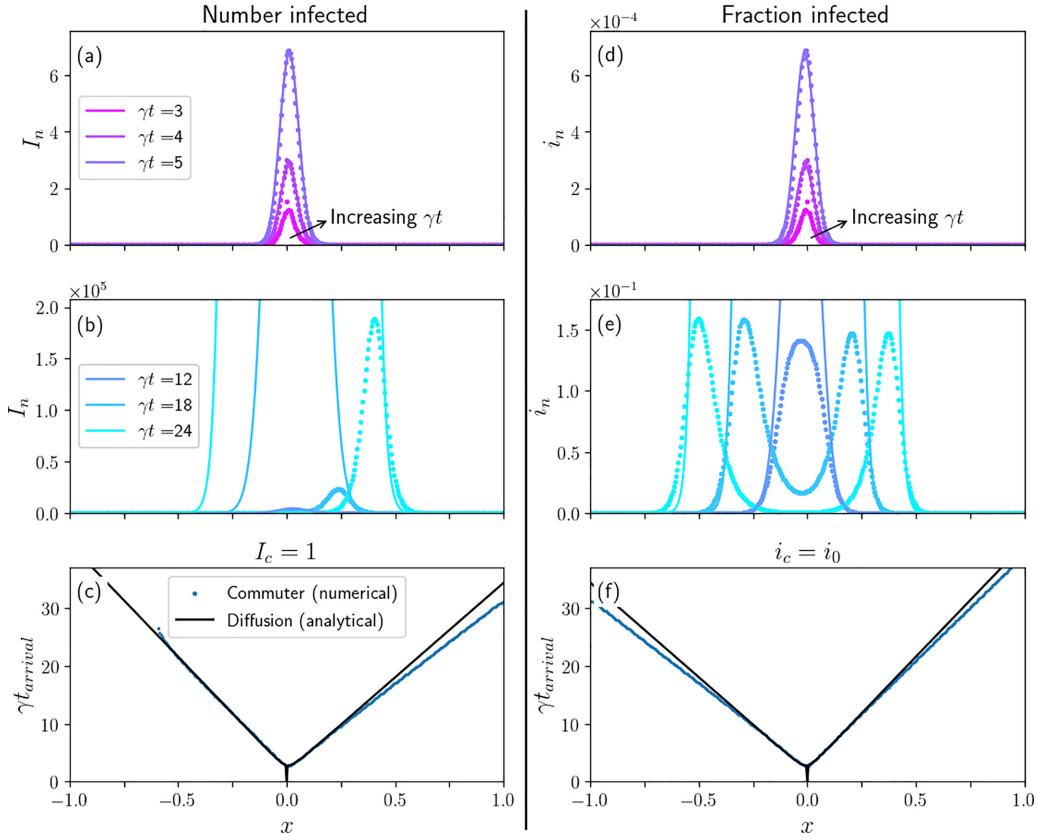
FIG. 3. Infection waves traveling in $d = 1$ from an initial infection at $x = 0$ in a nonuniform population $N_n = N_0 e^{x_n/\lambda_N}$ such that the drift velocity (35) is constant. In (a) and (b), the number of people infected at each location I_n is shown while in (d) and (e), the fraction of people infected at each location i_n is shown. The points are numerical solutions to Eq. (12b) with $G(|x|) \sim e^{-|x|/l}$, and the solid lines are analytical solutions to (38) multiplied by dx. Parameters used are $dx = 0.005$, $\sqrt{\langle x^2 \rangle} = \sqrt{2l^2} = 0.01$, $i_0 = 10^{-4}$, $R_0 = 2$, $N_0 = 10^4$, and $\lambda_N = 0.08$. (c) The smallest time that solves $I_n(t_{\text{arrival}}) \geqslant I_c$ is displayed for each location. Positive x values have a smaller arrival time, indicating that I_n drifts toward higher populations. (f) The smallest time that solves $i_n(t_{\text{arrival}}) \geqslant i_c$ is displayed for each location. Negative x values have a smaller arrival time, indicating that i_n drifts toward lower populations.

causes the infection density at the origin to increase, so there exists a finite time t^* at which the infection begins to increase. This places a lower bound on the offset time $t_O \geqslant t^*$. Solving $\dot{I}(0, t) = 0$ reveals a particularly simple form for this time:

$$t^* = \frac{d}{2} \frac{1}{\beta - \gamma}. \tag{41}$$

Assuming $R_0 > 1$, $I(0, t)$ increases for times greater than t^*, but $I(0, t)$ may still be less than the critical density. In these cases, $I(0, t)$ falls from infinity to below I_c at a time less than t^* and grows above I_c at a time greater than t^*. The time it takes to approach the critical density grows with the diffusion coefficient since this will lead to a broader spatial distribution of case counts at fixed total number of cases. It may be counterintuitive that high mobility increases the arrival time, but recall that we are assuming the total number of contacts a person makes is fixed, and D describes the spatial distribution of contacts. If contacts are only made between individuals in the same neighborhood (small D), then a local outbreak will quickly occur, but if the same number of contacts are distributed across a state (large D), then it will take much longer for any particular location to detect a severe

outbreak. In this way, the offset time should be thought of as the characteristic time it takes for the growth of the disease to dominate over the spread of the disease.

Before continuing our analysis, it will be useful to introduce a dimensionless quantity $\bar{l}$ characterizing this competition between growth and spread

$$\bar{l} \equiv \sqrt{\frac{d}{2e}} \sqrt{\frac{4\pi D}{\beta - \gamma}} \left(\frac{I_c}{I_0}\right)^{1/d} = \sqrt{\frac{2\pi}{e}} \sqrt{\frac{R_0 \langle x^2 \rangle}{R_0 - 1}} \left(\frac{I_c}{I_0}\right)^{1/d}. \tag{42}$$

Rewriting Eq. (38) in terms of $\bar{l}$,

$$\left[\frac{I(0, t)}{I_c}\right]^{2/d} = \frac{\exp t/t^*}{e\bar{l}^2 t/t^*}. \tag{43}$$

When we have $t_O > t^*$, the two solutions to $I(0, t) = I_c$ are given by solving the following transcendental equation:

$$-\frac{t}{t^*} e^{-t/t^*} = -\frac{1}{e\bar{l}^2}. \tag{44}$$

When $0 < \bar{l} < 1$, there is no real solution to the above equation, and we are in the regime where diffusion is small enough that $I(0, t)$ never falls below I_c. When $\bar{l} > 1$, there are two
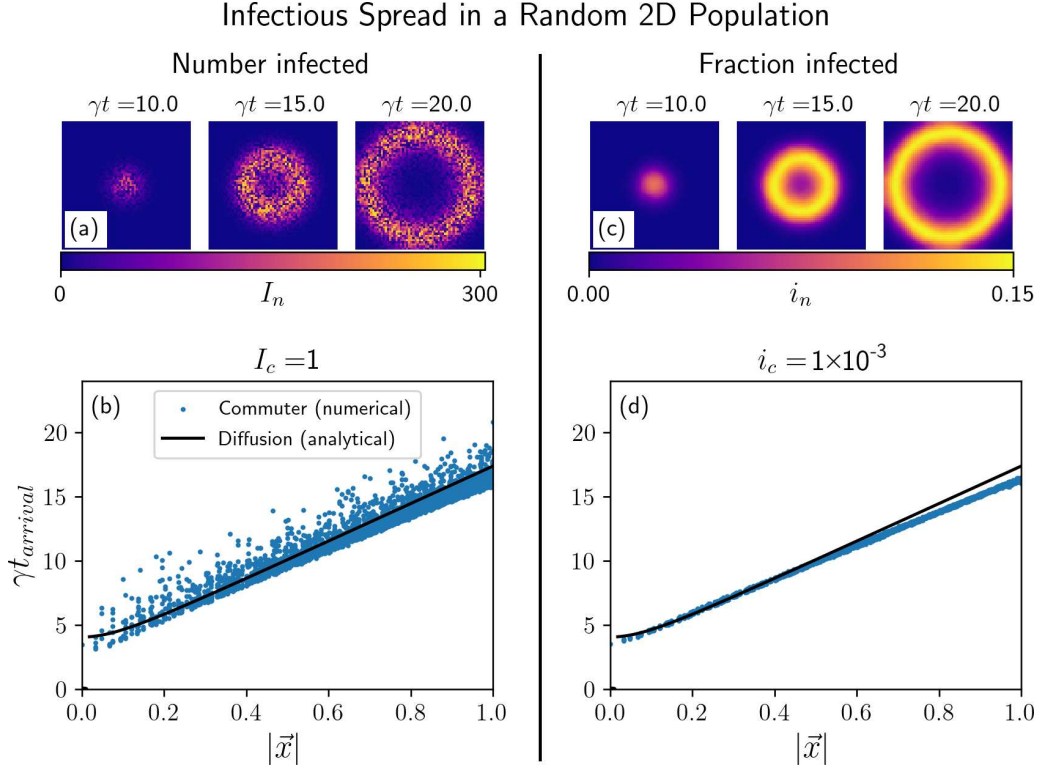
FIG. 4. Infection waves traveling in $d = 2$ from an initial infection at $\vec{x} = 0$ in a nonuniform population with N_n chosen from a uniform distribution between 0 and 2000. In (a), the number of people infected at each location I_n is shown for three different times while in (c), the fraction of people infected at each location i_n is shown for three different times. The points are numerical solutions to Eq. (12b) with $G(|\vec{x}|) \sim e^{-|\vec{x}|/l}$. The lattice is a 61 by 61 grid of side length $L = 2$, so $dx = 2/61$. Other parameters are $R_0 = 2$, $l = dx/2$, and $I_0 = 1$. (c) The smallest time that solves $I_n(t_{\text{arrival}}) \geqslant I_c$ is displayed for each location as a function of the distance from the origin $|\vec{x}|$. (d) The smallest time that solves $i_n(t_{\text{arrival}}) \geqslant i_c$ is displayed for each location. In either case, the numerical solution is compared to the analytic solution assuming $N_n = 1000$. Notice that the noise observed when considering I_n in (a) and (b) is eliminated when considering i_n in (c) and (d).

solutions (which converge to one solution for the special case $\bar{l} = 1$):

$$ t = \left\{ -t^* W_0\left(-\frac{1}{e\bar{l}^2} \right), -t^* W_{-1}\left(-\frac{1}{e\bar{l}^2} \right) \right\}. \quad (45) $$

Here W_k denotes the Lambert W function and k labels the branch cut. The first solution is the time at which $I(0, t)$ falls below I_c. The second solution is the offset time. Now we can explicitly write down the offset time for all values of $\bar{l}$:

$$ t_O = \begin{cases} t^*, & \bar{l} \in (0, 1) \\ -t^* W_{-1}\left(-\frac{1}{e\bar{l}^2} \right), & \bar{l} \in [1, \infty). \end{cases} \quad (46) $$

Looking at the form of $\bar{l}$, one can conclude that a reasonable choice of $\bar{l}$ will be greater than one. To see this, note that $\bar{l}^d > \sqrt{\langle x^2 \rangle}^d I_c/I_0$ which for $I_0 = 1$ can be interpreted as there being I_c sick individuals within the characteristic interaction volume. If this number were less than one, then the disease would not be detected, and this would be an inappropriately small choice of I_c. Therefore, for any reasonable definition of I_c, we will be in the regime $\bar{l} > 1$. When $\bar{l} > 1$, the offset time is inversely proportional to $(R_0 - 1)$ and grows monotonically with $\bar{l}$ as seen in Fig. 5.

Now that we know there is a finite time offset greater than t^* for reasonable choices of $\bar{l}$, we can expand the arrival time about the offset time and study the observed spatial spreading

patterns close to the origin. Plugging $t_{\text{arrival}} = t_O + \delta t$ into (39) and expanding to linear order in δt gives

$$ \delta t = \frac{1}{t_O - t^*} \left(\frac{|\vec{x}|}{c} \right)^2. \quad (47) $$

We also know that at large distances, the arrival time is $|\vec{x}|/c$. Using these two limiting behaviors, we can estimate the arrival time at all distances from the origin:

$$ t_{\text{arrival}}(\vec{x}) = t_O - \frac{t_O - t^*}{2} + \sqrt{\left(\frac{t_O - t^*}{2} \right)^2 + \left(\frac{|\vec{x}|}{c} \right)^2}. \quad (48) $$

Close to the origin, the infection is observed to spread diffusively, but far from the origin, waves form. The characteristic distance over which the spread transitions from diffusive to ballistic is $c(t_O - t^*)/2$. Interestingly, the arrival time close to the origin (as characterized by t_O) increases with $\sqrt{\langle x^2 \rangle}$, but the arrival time far from the origin (as characterized by $|\vec{x}|/c$) decreases with $\sqrt{\langle x^2 \rangle}$. Thus, long-distance commutes delay an outbreak in any one location because the interaction radius is increased, keeping the infection density everywhere low. However, once the exponential growth takes over, these low infection-density regions each spawn a local outbreak, and the disease is quickly detected throughout the whole domain. In the opposite limit, when commutes are short range, social mixing leads to a high infection density causing a quick
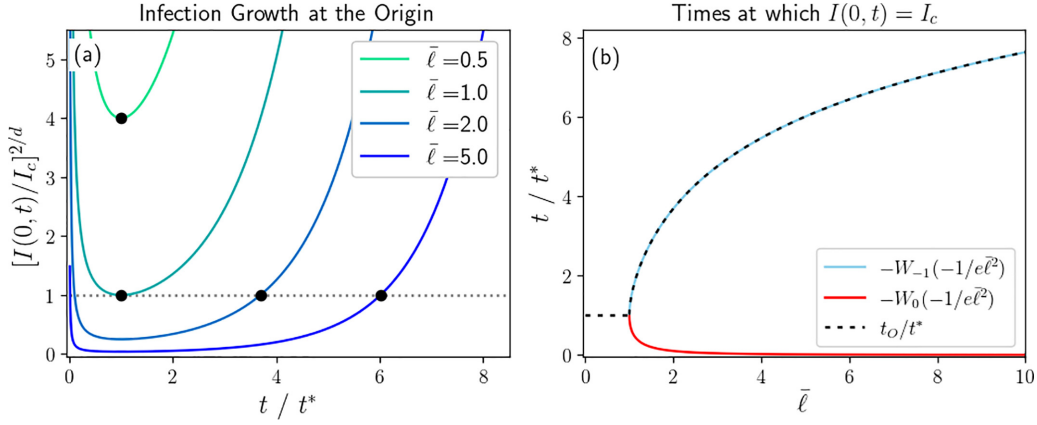
FIG. 5. (a) Solutions to (43) for different choices of $\bar{l}$ (colored lines). The dashed gray line is the line $I(0, t) = I_c$, and the black dots indicate the offset time. (b) The solid red (dark gray) and light blue (light gray) curves are the two solutions to Eq. (45), while the black dashed line is the normalized offset time (46). For $\bar{l} < 1$, $t_O = t^*$ which is the smallest time at which $\dot{I}(0, t) > 0$. For $\bar{l} > 1$, $t_O = -t^* W_{-1}(-1/e\bar{l}^2)$.

outbreak at the origin, but the propagation speed of the infection is slow, so it takes a while for the disease to be detected far from the origin.

2. Solutions in a finite domain

When our domain is bounded $\Omega = [-\frac{L}{2}, \frac{L}{2}]^d$, we will neither be able to assert that $\langle x^\mu \rangle = 0$ nor that $\langle x^2 \rangle$ is independent of position, but we can attempt to understand the boundary effects by using Eq. (36) along with Neumann boundary conditions (29). Physically, these boundaries could correspond to bodies of water or national borders.

If L is large enough and (21) is satisfied, then we expect to see infection waves, and the methods of the previous section can be used, but if L is small, then the infection quickly reaches the boundary before a wave can form, and the homogeneous dynamics (1) are recovered. We will only consider a uniform population in this section. Solving the linearization of (33) with boundary condition (29) and initial condition (37) gives

$$I(\vec{x}, t) = \frac{I_0}{L^d} \prod_{\mu=1}^{d} \sum_{n_\mu=-\infty}^{\infty} \cos\left(\frac{2\pi n_\mu x^\mu}{L}\right)$$
$$\times \exp\left[-D\left(\frac{2\pi n_\mu}{L}\right)^2 t\right] e^{(\beta-\gamma)t}. \tag{49}$$

In particular, for $\vec{x} = 0$ we get

$$I(0, t) = \frac{I_0}{L^d} \left[\sum_{n=-\infty}^{\infty} e^{-D(\frac{2\pi n}{L})^2 t}\right]^d e^{(\beta-\gamma)t}. \tag{50}$$

The spatial dependence decays away over a time $L^2/4\pi^2 D$, so if the arrival time is everywhere larger than or comparable to this value, the spread will appear to be homogeneous. It is worth mentioning that for $L^2/4\pi^2 D$ large, the terms in the sum change slowly, so one can turn the sum into an integral and recover Eq. (38).

In the previous section, we introduced the dimensionless commuting length $\bar{l}$ which parameterized the offset time in an infinite domain. Here we would like to introduce a second dimensionless length scale $\bar{L}$ to characterize the system size:

$$\bar{L} \equiv L\left(\frac{I_c}{I_0}\right)^{1/d}. \tag{51}$$

As mentioned in the previous section, reasonable choices of I_c will lead to the $\dot{I}(0, t) > 0$ condition automatically being satisfied (and a finite domain only reduces the time it takes to satisfy this condition), so let us assume we are at times after which $\dot{I}(0, t) > 0$. Then the offset time is given by solving $I(0, t_O) = I_c$:

$$\bar{L}^2 = \left[\sum_{n=-\infty}^{\infty} e^{-\pi e n^2 (\bar{l}^2/\bar{L}^2) t_O/t^*}\right]^2 e^{t_O/t^*}. \tag{52}$$

Equation (44) is recovered in the small $\bar{l}/\bar{L}$ limit where the sum can be converted to an integral. In the opposite limit of a well-mixed population (where we only keep the $n = 0$ term), the offset time is simply

$$t_O^{\text{WM}} \equiv t_O(\bar{l} \gg \bar{L}) = \frac{1}{\beta - \gamma} \ln\left(\frac{I_c L^d}{I_0}\right). \tag{53}$$

That is, a larger system (at fixed critical infection density) will have a larger offset time since there is more space for the infection to spread out. This limit gives the same result as the well-mixed population (5). In a well-mixed population, the entire population reaches I_c simultaneously, at which point $I_c L^d$ people are infected, which is necessarily greater than the initial number of people infected I_0, so we must have that $\bar{L} > 1$, and $t_O^{\text{WM}} > 0$.

One can check numerically that t_O/t^* is an increasing function of both $\bar{l}$ and $\bar{L}$. For moderate values of $\bar{L}$, the offset time resembles (46) for small values of $\bar{l}$ and resembles (53) for larger values of $\bar{l}$. Figure 6(a) demonstrates that the offset time can typically be estimated by one of these two simplified expressions, giving us a simple way of characterizing the
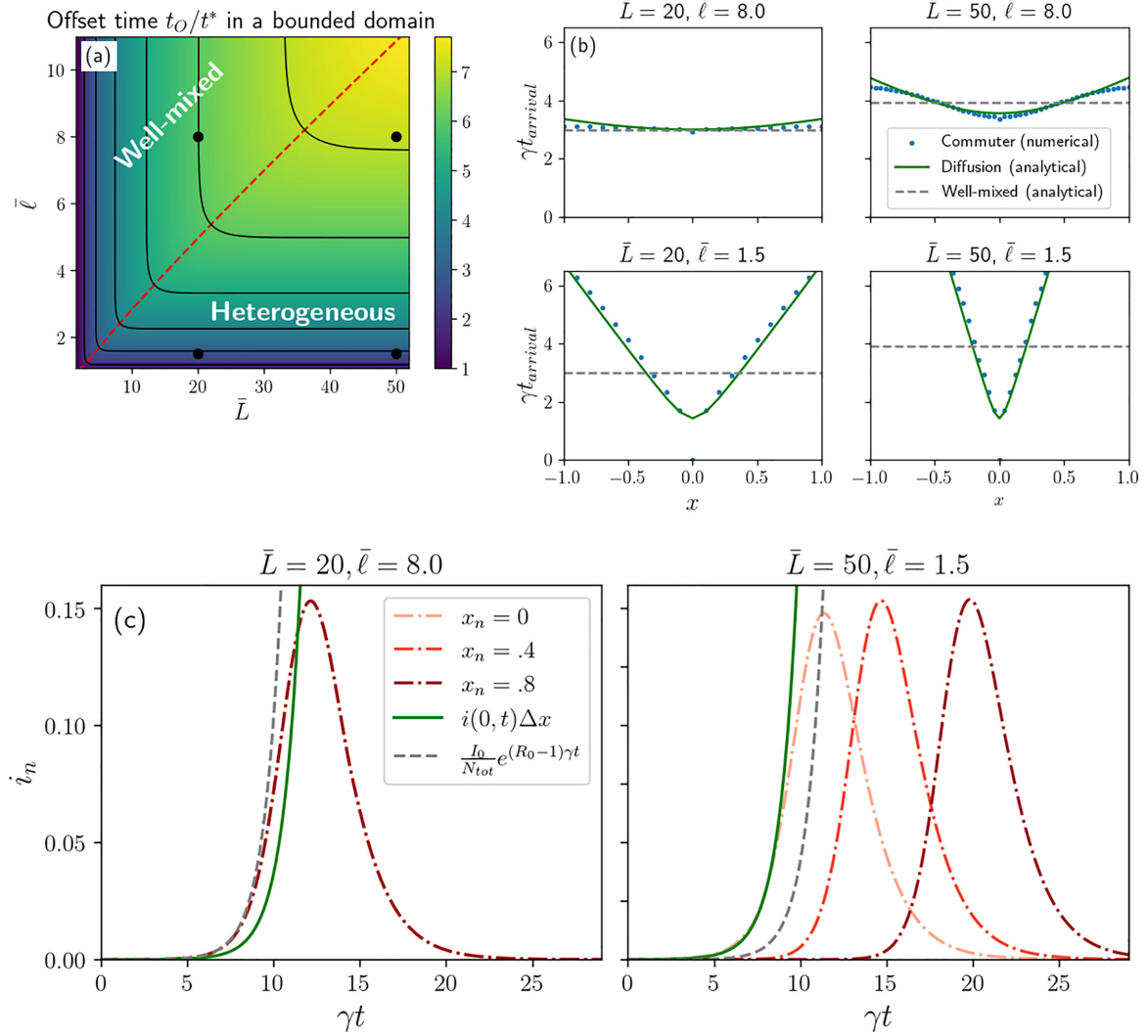
FIG. 6. Demonstration of finite-size effects on arrival time dynamics. (a) The theoretical time offset (52) is shown as a function of $\bar{L}$ and $\bar{l}$. In the top-left region, the contours are nearly vertical, indicating that the offset time only depends on system size, and (53) can be used; in the bottom-right region, the contours are nearly horizontal, indicating the offset time is independent of system size, and (46) can be used. The dashed line corresponds to Eq. (54), where the well mixed and $\bar{L} \to \infty$ solutions agree. In (b), the arrival time was found numerically by solving (12b) with $G(|\vec{x}|) \sim e^{-|\vec{x}|/l}$ in a uniform one-dimensional population of size $L = 2$, for different choices of $\bar{L}$ and $\bar{l}$ corresponding to the black dots in (a). $\bar{L}$ was varied by changing the step size while keeping I_c/I_0 fixed to $1/dx$. $\bar{l}$ was varied by changing the commuting length l. The green solid lines correspond to the analytical result in an infinitely large population satisfying (48) while the gray dashed lines give the well-mixed result (53). (c) Infection curves at different locations for an epidemic in the well-mixed regime (left) and an epidemic in the heterogeneous regime (right) are shown with dash-dotted lines of different shades. The green solid line shows the diffusion result (38), and the gray dashed line shows the solution to the linearization of (1b).

spreading dynamics as either heterogeneous or homogeneous (well mixed). By equating these two asymptotic expressions, we find that the transition occurs when

$$\ln(\bar{L}^2) = -W_{-1}\left(-\frac{1}{e\bar{l}^2}\right) \Rightarrow \bar{l}^* = \sqrt{\frac{1}{e}\frac{\bar{L}^2}{\ln(\bar{L}^2)}}. \quad (54)$$

That is, for $\bar{l} < \bar{l}^*$, the disease dynamics close to the origin can be approximated by those of the infinite system, and for $\bar{l} > \bar{l}^*$, the arrival time everywhere is approximated by the well-mixed result. Some sample arrival times calculated by solving (12) are shown in Fig. 6(b) and compared to the diffusion (48) and well-mixed results (53). Note that we could

have important boundary effects at positions away from the origin even when $\bar{l} < \bar{l}^*$. Some sample infection curves are shown in Fig. 6(c). In the well-mixed regime, the infection curves at different locations follow (4) with $i_{\text{tot}}(0) = I_0/N_{\text{tot}}$. In the heterogeneous regime, the infection curves separate in space, and the infection curve at the origin follows the diffusion model (38). One proposed way to capture the heterogeneity in disease spread is via an entropy function which measures the similarity of these infection curves at different locations [6]. However, this quantity requires knowledge of $i_n(t)$ for all n and t. What we have demonstrated is that simply looking at one location in space (the origin) at early times also characterizes the spreading behavior.

Even though we have given much attention to the offset time in cases where the diffusion approximation holds, we now understand the two most important limits. The smallest offset time corresponds to the case of a population with vanishingly small commuting range such that the infection density can quickly reach the threshold value. The largest offset time corresponds to a well-mixed population. Although $\bar{L}$ is defined for all commuting distributions, $\bar{l}$ is only defined for localized commuting distributions. What, then, do we expect for delocalized commuting distributions? The infection quickly reaches the boundary due to the divergent moments, so the more spread out the commuting distribution is, the closer the offset time will be to the well-mixed prediction. In general, the well-mixed result gives an upper bound to the offset time: $t_O \leqslant t_O^{\text{WM}}$.

B. Localized commuting beyond the diffusion approximation

1. Exact calculation of the wave speed

When truncating our Taylor series to quadratic order, we found a reaction-diffusion system. This should work well at small values of x, but at larger values of x, the higher-order derivatives will, in general, matter. Therefore, we might expect that the calculation of the time offset (which is defined at the origin) should work well under the diffusion approximation provided $\langle x^2 \rangle$ is finite. However, the wave speed should be calculated far from the origin, where the diffusion approximation is no longer expected to work. Although the diffusion approximation correctly predicts the existence of waves, we need a new tool to quantitatively predict the wave speed for a given contact distribution. Mollison showed that for the special case of an exponential contact distribution, the exact wave speed can be calculated [26] and has a noticeable deviation from the result obtained from the diffusion approximation. Later, Daniels generalized the result to show how to calculate the wave speed for any localized contact distribution by using moment-generating functions [38]. Here we will apply the technique of moment-generating functions to the commuter model. We have a few probability distributions to choose from, but the most relevant for the dynamics will be the commuter distribution $G(|\vec{x}|)$ and the contact distribution $\beta(\vec{x}, \vec{y})$. Consider two related quantities:

$$\phi(\vec{k}) = \int e^{\vec{k} \cdot \vec{x}} G(|\vec{x}|) d^d x, \tag{55}$$

$$\psi(\vec{k}, \vec{x}) = \beta^{-1} \int e^{\vec{k} \cdot (\vec{y} - \vec{x})} \beta(\vec{x}, \vec{y}) d^d y. \tag{56}$$

When the population is uniform, $\psi(\vec{k}, \vec{x}) = \psi(\vec{k})$, and we have the simple relationship $\psi(\vec{k}) = \phi(\vec{k})^2$. Plugging the ansatz $i(\vec{x}, t) \sim e^{\vec{k} \cdot (\vec{x} - \vec{c} t)}$ into (26) with $s(\vec{x}, t) = 1$ and assuming a uniform population gives a constraint on $c(\vec{k})$:

$$c(\vec{k}) = \frac{\beta \phi(\vec{k})^2 - \gamma}{|\vec{k} \cdot \hat{r}|}. \tag{57}$$

For a localized initial condition like we have been considering, the correct choice of $\vec{k}$ is that which minimizes $c(\vec{k})$. Note that

the diffusion approximation considered previously amounts to keeping only quadratic terms in our moment-generating function. If we make the approximation $\phi(k) \approx 1 + \frac{1}{2d} k^2 \langle x^2 \rangle \Rightarrow \phi(k)^2 \approx 1 + \frac{1}{d} k^2 \langle x^2 \rangle$, then one can easily check that the minimum wave speed is that given in Eq. (40). In order to find the nonperturbative wave speed, one must first find the exact moment-generating function $\phi(\vec{k})$ and then find the minimum of (57) numerically.

As an example, let us find $\phi(\vec{k})$ and $c(\vec{k})$ in one dimension (1D) when G takes the form of Eq. (16). For $|kl| < 1$,

$$\phi(kl) = (1 + kl)^{p-1} e^{+klr_0/l} \frac{\Gamma(-(p-1), (1+kl)r_0/l)}{2\Gamma(-(p-1), r_0/l)}$$
$$+ (1 - kl)^{p-1} e^{-klr_0/l} \frac{\Gamma(-(p-1), (1-kl)r_0/l)}{2\Gamma(-(p-1), r_0/l)}, \tag{58}$$

where $\Gamma(s, x)$ denotes the incomplete Gamma function

$$\Gamma(s, x) = \int_x^\infty w^{s-1} e^{-w} dw. \tag{59}$$

Taking the limit $r_0/l \to 0$ is difficult, especially when p is a positive integer, but intuitively, as $r_0/l \to 0$, $G(|\vec{x}|)$ becomes sharply peaked at $\vec{x} = 0$, so $\phi(kl) \approx 1$. Although the kl dependence is important if we want to find any nonzero moments, taking $\phi(kl) = 1$ actually gives us a good estimate for c. In that case, the minimum value of c occurs when $|kl| = 1$ (a strong indication that our diffusion approximation will fail), and the minimum speed is equal to $(R_0 - 1)l$, unlike that predicted by Eq. (40). Unsurprisingly, the speed becomes infinite for a power law ($l = \infty$) since we no longer satisfy Eq. (21). Setting $\phi(kl) = 1$ fails when $p \ll 1$ where the distribution becomes exponential and $\phi(kl) \approx \frac{1}{2}[(1 + kl)^{p-1} + (1 - kl)^{p-1}]$. Notably, when $p = 0$ (exponential distribution), we have $\phi(kl) = \frac{1}{2}[1 - (kl)^2]^{-1}$, and c is slightly greater than that predicted by the diffusion approximation, consistent with the small discrepancy in the arrival times shown in Fig. 2. The moment-generating functions and wave speeds for various choices of p and r_0/l are shown in Fig. 7. When a truncated power law with a small length scale is used, there is an even larger disagreement with the diffusion approximation. The key takeaway is that even though the Taylor series is valid for any localized commuting distribution, keeping only the quadratic terms fails to predict the correct wave speed, and higher moments should be considered. Even more effects absent from the reaction-diffusion system can be found when $N(\vec{x})$ is nonuniform, as will be explored in the next section.

2. Fourth-order corrections to the reaction-diffusion system

Returning to the calculation performed to obtain the reaction-diffusion system, here we will instead Taylor expand $i(\vec{z}, t)$ and $N(\vec{z})$ to fourth order. The calculation is tedious, so we only give the result for 1D, where primes denote spatial derivatives, and all quantities on the right-hand side are
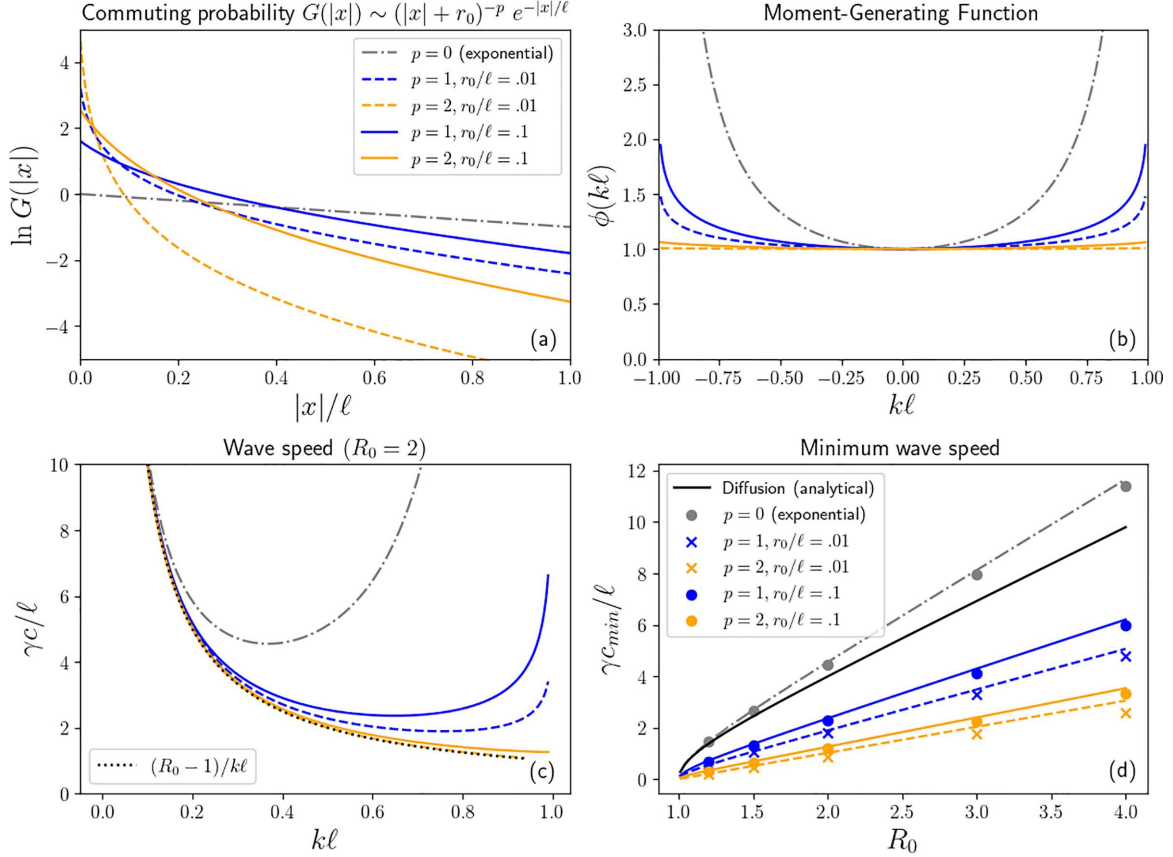
FIG. 7. Demonstration of how to calculate the infection wave speed of a general localized contact distribution. (a) Truncated power-law commuting distributions and (b) their corresponding moment-generating functions as given by Eq. (58) for various powers p and length scale ratios r_0/l. (c) Wave speed for each kl at a fixed R_0, as predicted by Eq. (57). The physical wave speed is the minimum speed on this curve. (d) Curves are generated by minimizing (57) over all kl for different choices of R_0. The circles and crosses denote values obtained numerically by finding the slope of the arrival time far from the origin. The numerical results are compared to the diffusion result (40) shown with a black line.

evaluated at x,

$$\int dy \frac{\int dz\, P(z,y)N(z)i(z,t)}{\int dz\quad P(z,y)N(z)} \approx i + \left(i'' + \frac{N'}{N}i'\right)\langle x^2\rangle + \left\{\frac{1}{12}i'''' + \frac{1}{6}\frac{N'}{N}i''' + \left[\frac{1}{2}\zeta(\zeta-1)\frac{N'^2}{N^2} + \frac{1}{4}\frac{N''}{N}\right]i''\right.$$

$$+ \left[-\frac{1}{2}\zeta(\zeta-1)\frac{N'^3}{N^3} + \zeta(\zeta-1)\frac{N'N''}{N^2} + \frac{1}{6}\frac{N'''}{N}\right]i'\right\}\langle x^4\rangle$$

$$+ \left\{\frac{1}{4}i'''' + \frac{1}{2}\frac{N'}{N}i''' + \left[\left(-\frac{5}{4}\zeta^2 + \frac{9}{4}\zeta - 1\right)\frac{N'^2}{N^2} + (1-\zeta)\frac{N''}{N}\right]i''\right.$$

$$+ \left[(1-\zeta)(1-2\zeta)\frac{N'^3}{N^3} + \left(-4\zeta^2 + \frac{13}{2}\zeta - 2\right)\frac{N'N''}{N^2} + \left(-\zeta + \frac{1}{2}\right)\frac{N'''}{N}\right]i'\right\}\langle x^2\rangle^2. \quad (60)$$

The first line is the diffusion result, but the numerous other terms are new. The higher-order N-independent terms correct the wave speed as shown in the last section. The $\langle x^2\rangle^2$ terms involve second-order processes which we would not have obtained by considering only dynamics where either the susceptible or the infected travel. We now see terms which depend on ζ. While this equation is too complicated to say exactly how ζ changes quantities like the arrival time, we can

see a few things. Because the ζ terms all involve at least two derivatives of N and factors of the characteristic commuting distance to the fourth power, in order for these terms to be non-negligible, we need N to change on length scales comparable to the characteristic commuting length. If the population changes on much greater length scales, then the dominant effect will be the N'/N term (which may also be negligible). If the population changes on much smaller length scales, then
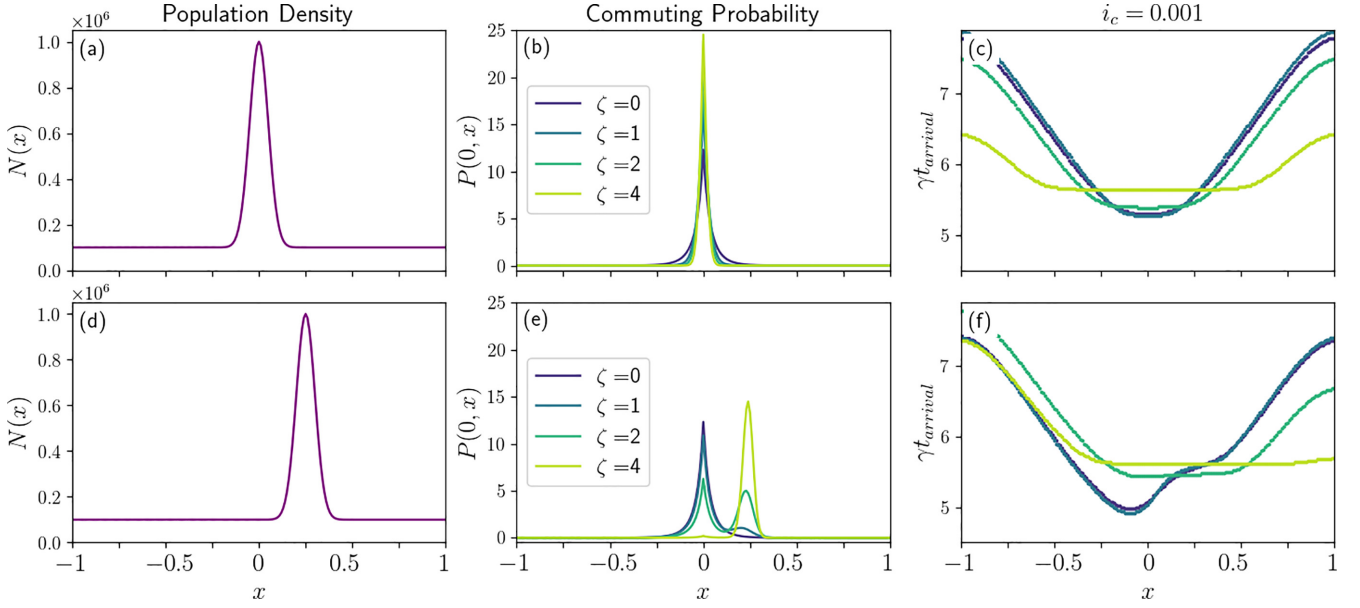
FIG. 8. Demonstration of the ζ dependence in the continuous commuter model. (a) A Gaussian population profile was chosen whose center lies at the origin: $N(x) = 10^5 + 9 \times 10^5 e^{-x^2/2\lambda_N^2}$. (b) Commuting probabilities of the form $P(0, x) \sim N(x)^\zeta e^{-|x|/l}/(|x| + r_0)^2$. The probability for an individual living at the origin to travel to the city is larger for higher ζ, reducing the arrival time near the city. (c) Arrival times obtained by numerically solving (12b). The presence of the city leads to more homogeneous dynamics when ζ is increased. Parameters used were $l = 0.1$, $r_0 = 0.1$, $\lambda_N = 0.05$, $R_0 = 2$, $I_0 = 1$, $dx = 0.01$, $L = 2$. In (d)–(f), the simulation is repeated except the city is shifted to the right: $N(x) = 10^5 + 9 \times 10^5 e^{-(x-.25)^2/2\lambda_N^2}$. In either case, the infection was initialized at the origin.

the population fluctuations can be averaged over as already shown. See Fig. 8 for an example population where the ζ-dependence is important. First, notice that larger values of ζ lead to more homogeneous dynamics, a phenomenon which will be explained by Eq. (61). Next, notice in the bottom row that although the drift term would cause the infection to travel left toward lower populations (when plotted in terms of i_n), the higher-order terms drive the infection toward the city for larger values of ζ. Finally, notice that the arrival times for $\zeta = 0$ and $\zeta = 1$ are nearly indistinguishable. Looking at the above equation, we see that all of the terms proportional to $\langle x^4 \rangle$ are identical for $\zeta = 0$ and $\zeta = 1$. It is not clear why we have this symmetry, but this manifests itself in our simulations where it is often hard to distinguish between commuting populations with $\zeta = 0$ and $\zeta = 1$.

C. Continuous commuter model results: Most general case

The previous two sections have focused on two extreme limits: If the system is small or commuters travel long distances, then the well-mixed dynamics (1) are recovered, but if the travel probabilities fall off exponentially and the system size is large enough, a reaction-diffusion system approximates the dynamics. In either of these two limits, the precise form of the commuting probabilities is unimportant (only $\langle x^2 \rangle$ matters to leading order). Our first indication that the precise commuting patterns matter shows up at fourth order in our Taylor series, as shown in the previous section. This hints at the fact that the most interesting dynamics happen for commuting distributions which are delocalized so the reaction-diffusion system fails but also not too long ranged as to lead to homogeneous dynamics. So far, we have only studied cases where

(21) is satisfied such that our Taylor series is valid (even if it may require us to go to higher orders). In this section, we relax that assumption and study the role of ζ and G for general commuting probabilities $P(\vec{x}, \vec{y}) \sim N(\vec{y})^\zeta G(|\vec{x} - \vec{y}|)$.

Let us first study the role of G in a uniform population. See Fig. 9. Three choices of G were chosen, all with the same $\langle x^2 \rangle$ and thus the same diffusion coefficient. The Gaussian, exponential, and power-law commuter distribution all show an arrival time quadratic in position close to the origin with the same time offset. At later times, the Gaussian and exponential commuter distributions give rise to waves approximated by (40), but the power law does not, consistent with (21). The diffusion approximation seems to hold at small distances even for the power law with $p = 4$ (in this case $\langle x^2 \rangle$ is finite), but because the higher-order moments diverge for the power law, the diffusion solution fails at larger distances. This rapid spread of infection for delocalized distributions is characterized by a sublinear arrival time. The fact that the offset time is the same for these three commuting distributions despite the power law behaving differently suggests that not all of the spreading dynamics can be captured by the offset time alone. One can compare the results from the power law to a completely delocalized contact distribution $G = 1/L$ where the arrival time is constant and given by the time offset (53).

Despite the variety of solutions predicted by different choices of G, we expect infectious spread to be no faster than the well-mixed results and no slower than the diffusion results at a comparable $\langle x^2 \rangle$, when it is defined. This idea is explored further in Fig. 10(a) where several different power-law commuting distributions with the same $\sqrt{\langle x^2 \rangle}$ give the same offset time and early time dynamics, but far from the origin, the larger values of p have larger arrival times. For
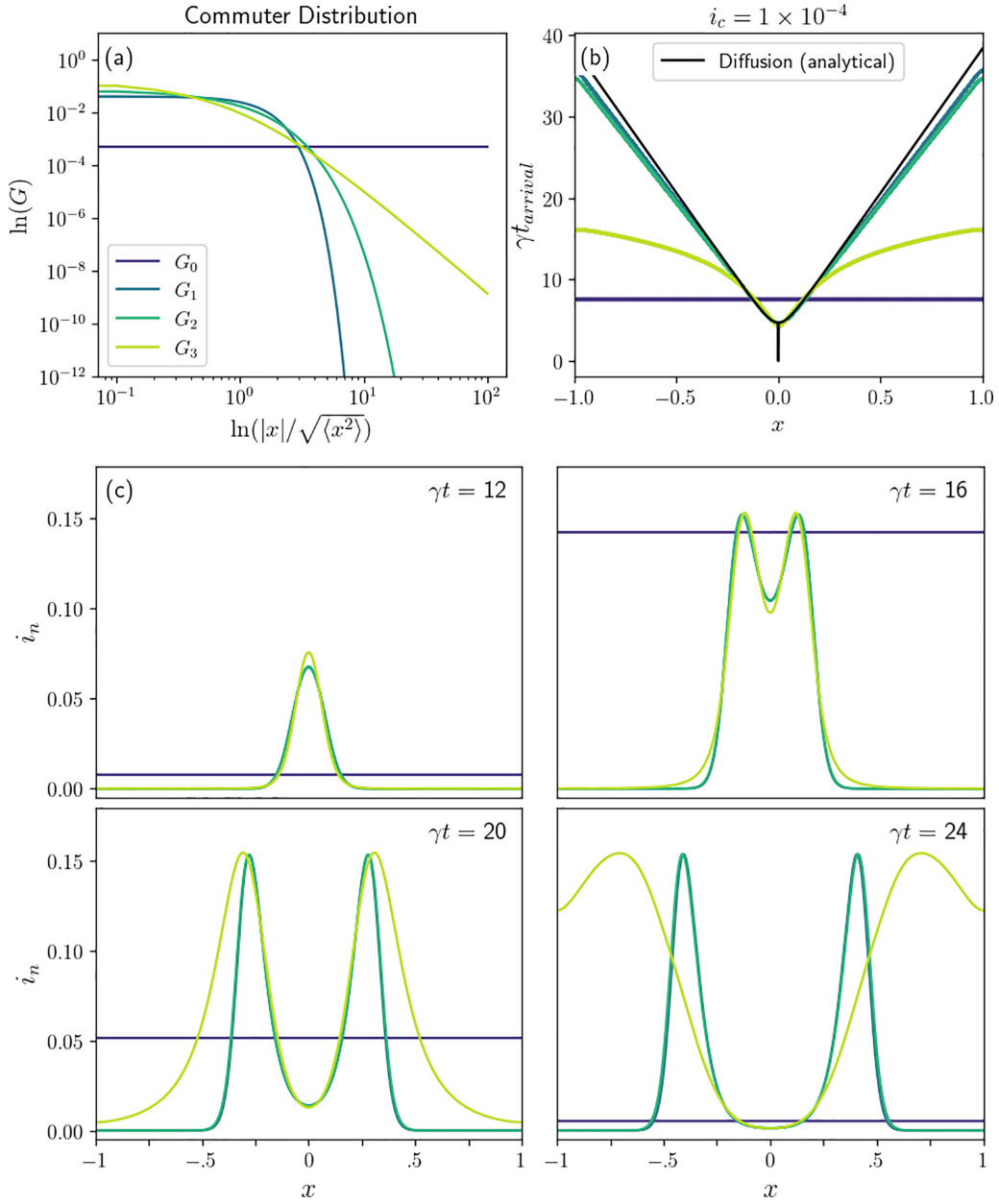
FIG. 9. Numerical results for the 1D homogeneous commuter model for four different choices of G: completely delocalized $G_0(x) = \frac{1}{L}$, Gaussian $G_1(x) = \frac{e^{-x^2/2\langle x^2 \rangle}}{\sqrt{2\pi \langle x^2 \rangle}}$, exponential $G_2(x) = \frac{e^{-|x|/\sqrt{\langle x^2 \rangle/2}}}{2\sqrt{\langle x^2 \rangle/2}}$, and power law $G_3(x) = \frac{3}{2\sqrt{\langle x^2 \rangle}}(1 + \frac{|x|}{\sqrt{\langle x^2 \rangle}})^{-4}$. (a) Commuter distributions plotted on a log scale. Note that the value of $\sqrt{\langle x^2 \rangle}$ was fixed to be the same for G_1, G_2, and G_3. (b) The arrival times for each commuter distribution were found. The Gaussian and exponential distributions give rise to a linear arrival time far from the origin, consistent with the diffusion result shown in black. The power law initially resembles the diffusion result, but becomes sublinear far from the origin. Despite having the largest time offset, the completely delocalized distribution has the smallest arrival time far from the origin. (c) Four time snapshots of the infection dynamics for each commuter distribution. The power law displays an accelerating infection front. Parameters used were $dx = 0.001$, $\sqrt{\langle x^2 \rangle} = 0.01$ (for G_1, G_2, G_3), $L = 2$, $i_0 = 10^{-4}$, and $R_0 = 2$.

$p \leqslant 3$ in 1D, $\sqrt{\langle x^2 \rangle}$ is undefined, but we can instead fix the length scale r_0 in Eq. (16) (with $l \to \infty$). See Fig. 10(b). For $p \leqslant 1$, the commuting distribution is not normalizable in 1D, so the dynamics are homogeneous. For $1 < p \leqslant 3$, all moments diverge, and the offset time is noticeably larger while the arrival times at long distances are small. Larger

values of p have a smaller time offset but arrive later at large x.

To investigate the role of ζ for delocalized distributions, we will look at a two-dimensional nonuniform population and try different power laws and values of ζ. Numerical results are shown in Fig. 11. For $p \leqslant 4$, $\langle x^2 \rangle$ diverges in two dimensions,
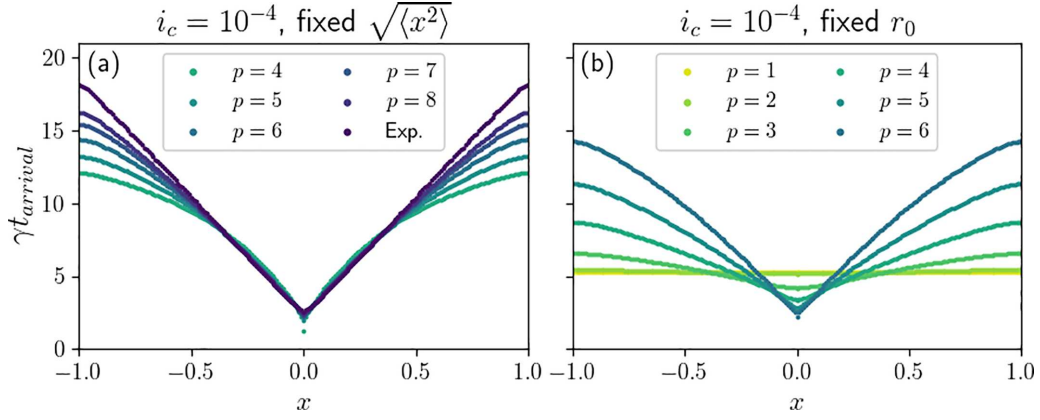
FIG. 10. Arrival times for different power-law commuter distributions $G(x) \sim (|x| + r_0)^{-p}$. In (a), r_0 was chosen for each p to fix $\sqrt{\langle x^2 \rangle} = 0.02$ using $r_0(p) = \sqrt{(p-2)(p-3)\langle x^2 \rangle / 2}$. In (b), $r_0 = 0.05$ was fixed. Additional parameters used were $dx = 0.01$, $i_0 = 0.0001$, and $R_0 = 2$.

so the arrival time grows slower than x. For $p = 3$, some spatial dependence can be seen for small values of ζ, but the dynamics are still nearly homogeneous. A symmetry appears to exist between the $\zeta = 0$ and $\zeta = 1$ cases for all values of p

studied, as we saw for the localized case. The case $\zeta = 2$ and $p = 4$ is the most interesting. The infection fraction increases along the line connecting the origin to the city but grows slowest on the side of the city opposite the origin, producing
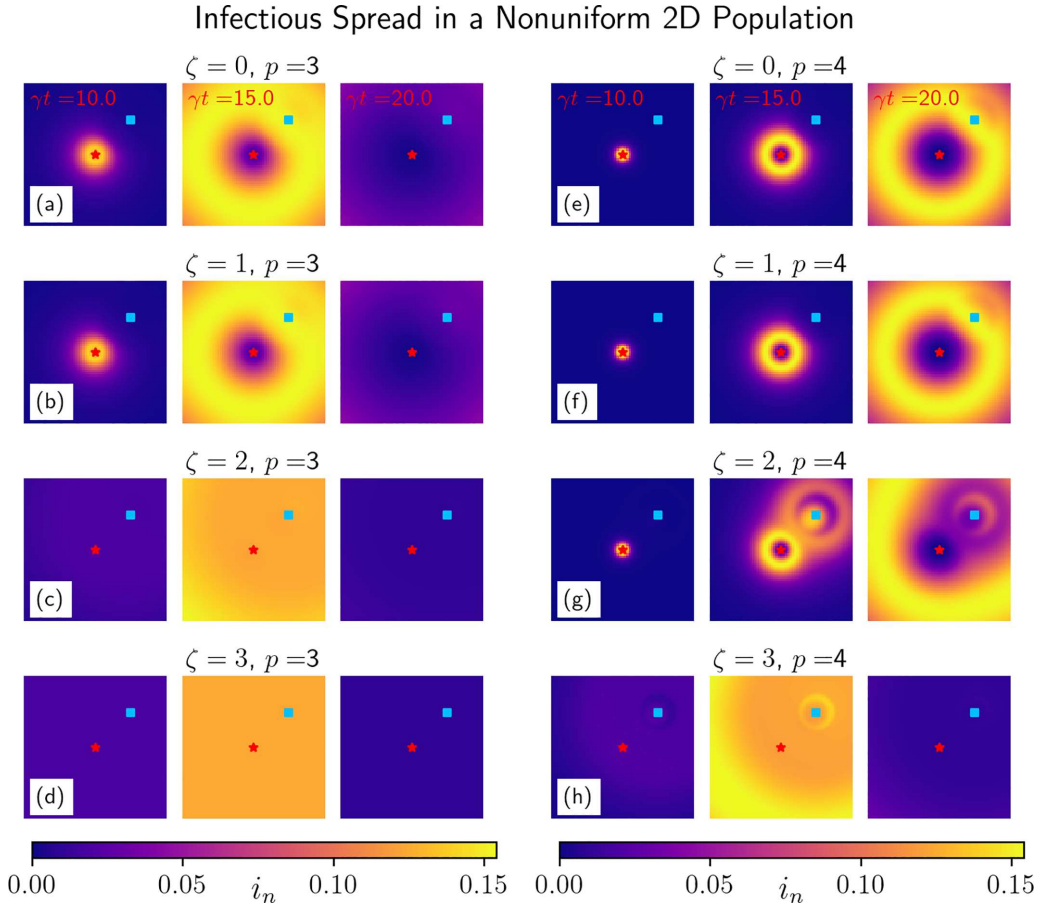

FIG. 11. Simulations using a commuting probability $P_{nm} \sim N_m^\zeta (|\vec{x}_n - \vec{x}_m| + r_0)^{-p}$ for different choices of ζ and p with $N_m = 100 + 9900 \exp -|\vec{x}_m - (0.5, 0.5)|^2 / \lambda_N^2$ such that there is a city located in the northeast (blue square) with population 100 times larger than elsewhere in the domain. A single infected person is introduced at the origin (red star) at $t = 0$. For each choice of ζ and p, three time snapshots of the infection fraction are shown. Panel (g) demonstrates a new phenomenon where the infection fraction first increases in the city and then spreads away from the city. This behavior is not predicted in the diffusion approximation or the well-mixed approximation. The lattice is a 61 by 61 grid with side length $L = 2$, so $dx = 2/61$. Other parameters are $R_0 = 2$, $r_0 = dx/4$, $\lambda_N = 0.05$.

a visible eclipse in the infection fraction. This can roughly be understood as a competition between two effects. $I(x, t)$ drifts toward the city from the origin as more people travel to the city to go to work than elsewhere, but there is the additional factor of $1/N(x)$ which reduces $i(x, t)$ close to the city. Once the infection reaches the city, there is a rapid spread from the city to the boundary. This observation that cities can act as disease amplifiers was also seen in Ref. [10], where the commuting probability was taken to be the sum of a localized term and a delocalized term.

For large-enough values of ζ for any p, the spreading appears homogeneous. To understand this, note that if N_m has a unique maximum at $m = M$ and $G(|\vec{x}_m - \vec{x}_n|)$ is everywhere nonzero, then

$$\lim_{\zeta \to \infty} P_{nm} = \delta_{mM} \Rightarrow \lim_{\zeta \to \infty} \sum_k \beta_{nk} i_k = \beta \frac{I_{\text{tot}}}{N_{\text{tot}}}, \qquad (61)$$

which means, for large ζ, the entire population meets at the high-population hub where it is equally likely for someone to meet anyone else in the population, so the well-mixed equations (1) are recovered. Typically we think of a well-mixed population as one where individuals travel everywhere, yet here, we see the emergent dynamics are the same if all commuters travel to one central location. In this limit, most interactions are second order, so we will not see this effect using the simplified commuter interactions (14) nor would this limit make sense in a Eulerian model. Although taking the limit $\zeta \to \infty$ seems unphysical, Fig. 11 suggests that we do not need to make ζ too large to observe this effect.

Little is known about epidemic models with delocalized contact distributions. Brockmann suggests that these cases can be modeled with fractional diffusion equations [22]. Some effort has been made to characterize the front dynamics in models with growth and fractional diffusion [44,45], but little effort has been made to characterize the subtle arrival time properties we have seen here. Hallatschek and Fisher studied the arrival times in a stochastic model where individuals jump to a particular location according to some delocalized jump distribution [46]. The model predicted accelerating fronts with distinct arrival time scalings depending on the power law of the jump distribution. Our model is distinct from these models in that our model incorporates Lagrangian movement patterns. A detailed analysis of delocalized commuting in an epidemic model (to the level that we were able to do for the localized commuter distributions) is still an open problem.

IV. DISCRETE RESULTS

Now that we understand the commuter model in the continuum, we would like to apply the model on a map using real geographic and census data. First, we will demonstrate new subtleties that arise when relaxing the assumptions of infinitesimal county size and uniform county shape. Then the theory will be applied to a couple realistic commuting distributions. Previous papers have integrated human mobility models and epidemic models on maps using a primarily data-driven approach [1,5,7,10]. Here we demonstrate that the theoretical features we have studied so far can persist when applied to real geographic regions, without the intention to directly compare with data for a specific epidemic.

A. Commuters on a nonuniform grid

Let us work in the limit where the discreteness of the lattice is apparent. When the step size is larger than the characteristic commuting length, the diagonal entries of **P** dominate, so the infection spreads slower than the results obtained by diffusion. See Fig. 12(a). The offset time is reduced because a larger step size means the growth term dominates the diffusion term early. Note that the value of $\langle x^2 \rangle$ used for the analytical result is that obtained from the continuous function $G(|\vec{x}|)$. Infection waves are still observed at late times but with a speed less than (40).

An additional complication which arises on maps is that counties may all be different sizes. Because the distance to the center of a neighboring county with smaller area will be less than the distance to the center of a neighboring county with larger area, the probability to travel to a smaller county will be greater. This effect is demonstrated in Fig. 12(b) where a nonuniform county spacing causes the disease to drift rightward.

These complications highlight the care that one must take when applying the model to maps. Unlike some biological systems where discreteness is a relevant feature that leads to interesting spreading phenomena [41], the spread of disease should not depend on county borders, so these effects must be artificial. The problem arises because the commuting distribution is defined in continuous space $G(|\vec{y} - \vec{x}|)$, but the populations (N_n, I_n, etc.) are defined for discrete systems. In order to construct the commuting probabilities between counties, we assumed the form (15) where $\vec{x}_n, \vec{x}_m$ are the county centers. This is a good estimate when Δx is small, but in cases where Δx is large, our expressions should involve integrals over the county area. There are two solutions. Of course, if the commuting probabilities or commuting fluxes between counties are known, then guessing a form such as (15) is unnecessary, and solving the discrete model (11) is appropriate. For the purposes of our theory where we are investigating the role of different gravity models, one can coarse grain the populations so that the continuum approximation holds, find the density fields using (26), then integrate the fields over the county area to obtain S_n, I_n, R_n. In the next section, when we apply the model to the United States, we find the qualitative results of our continuum theory to hold when naively applying (15), so at the cost of not getting quantitative agreement with our analytic results, we will use the simpler approach of evaluating the commuting probability at the center of population of each county.

B. Commuters on a map

We simulate the commuter model on a map of the United States with realistic populations and county geometries. Population data was obtained from the U.S. Census Bureau [47]. Geometric data were retrieved from Plotly [48] and visualized using the GeoPandas package of Python. The coordinate $\vec{x}_n$ of a given county is taken to be the center of population. Given the latitudes $\{\theta_n\}$ and longitudes $\{\phi_n\}$ of each county center in
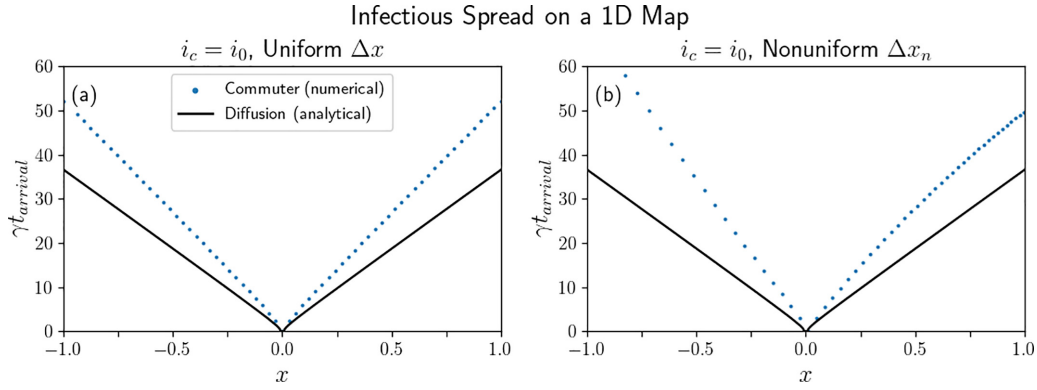
FIG. 12. (a) Arrival times in $d = 1$ using the same parameters as in Fig. 2, except $\Delta x = .03 > l$ such that the continuum theory (black line) fails. (b) The county spacing Δx_n is taken to be nonuniform: $\Delta x_n = (\Delta x)e^{-4x_n/3L}$ such that the continuum theory fails and the infection reaches smaller counties earlier.

radians, the separation between two counties is approximated as

$$|\vec{x}_m - \vec{x}_n| \approx R_E \sqrt{(\theta_m - \theta_n)^2 + \cos^2\left(\frac{\theta_m + \theta_n}{2}\right)(\phi_m - \phi_n)^2}.$$

(62)

The first set of parameters we will try is that obtained by Balcan *et al.* [1], who performed a Voronoi tessellation based on distance from major airports to divide the United States into units more suitable for studying mobility processes. They found that the commuting distribution takes the form of an exponential with a decay length of $l = 51$ miles (for distances not too large). We will try applying this commuting distribution at the county level, though it is worth noting that because the spatial units considered in their paper were larger than a typical U.S. county, this may be an unrealistically large l for our purposes. The commuting distribution and resulting contact matrix elements are visualized in Figs. 13(a) and 13(b). Broad infection waves are shown in Fig. 13(c). Even though l is large, Fig. 13(d) shows that the arrival time still resembles that predicted by the reaction-diffusion system: a finite offset followed by a quadratic regime and finally a linear regime. Also, notice that even though the commuting probability is asymmetric due to the nonuniform population distribution in the U.S., the arrival time changes smoothly, as observed by the smooth gradient in the colors of Fig. 13(e).

Now we will consider the parameters obtained from county workflow data by Viboud *et al.* [49]. They found a power-law fit for the commuting distribution with $p = 3.05$, and the tendency to travel to cities is given by the exponent $\zeta = 0.64$ (which is, interestingly, identical to the value that Balcan found [1]). Results are shown in Fig. 14. The arrival time is sublinear and has a larger variance. As expected with delocalized commuting distributions, the disease travels faster than any wave, and complex population-dependent behavior emerges.

These two examples demonstrate that although some human mobility processes can seemingly be described by either an exponential distribution or a power law, the emergent infection dynamics will differ greatly. This claim is even stronger when comparing commuter distributions with smaller length

scales, as shown in Fig. 15. At $\gamma t = 15$, the epidemic appears more severe close to Dallas for the localized distribution [Fig. 15(a)] due to the smaller time offset, but by $\gamma t = 20$, the infection has spread across the entire country for the delocalized distribution [Fig. 15(b)], while the infection spreads as a wave for the localized distribution. In either case, the final fraction of individuals who were at some point infected was found to be $r_{tot} = 0.797$, identical to that predicted by (3), as expected.

V. DISCUSSION

Even in our globalized world, commuting patterns play an important role in shaping disease spread. During the beginning of the COVID-19 pandemic in early 2020, commuting flows helped to explain the spread of disease from its source in Wuhan, China [9]. Spatiotemporal data in Italy suggest that the infection traveled along highways [11]. Recent work showed that metapopulation models can be used to quantitatively describe the spread of SARS-CoV-2 [8,50]. These metapopulation models are closely related to the classic papers on disease propagation [16,17,26] but possess new challenges. Little work has been done to bridge the gap between the more data-driven metapopulation models and the theoretical results derived in mathematical epidemiology. One work made this connection in the Eulerian formalism [22], less appropriate for incorporating commuter dynamics. These Eulerian movement models have been more useful for deriving effective metrics used to characterize the arrival times of a disease on a network [5,13], but infection dispersal due to commutes gives rise to behaviors that are best studied in real space using a Lagrangian movement model where individuals have a well-defined home. While Lagrangian movement for commuters has been incorporated into epidemic models [7,8,10], these works focus on contact matrices derived from known commuting patterns of specific regions. Here we studied a broad class of models that incorporate more general principles from human mobility theory [35,37].

Two commonly studied limits were obtained from our model. When the commuting distribution has an exponential tail and the domain is large enough, the infection is initially localized near the source and the spread is diffusive, but at later times, traveling infection waves can be observed. If the
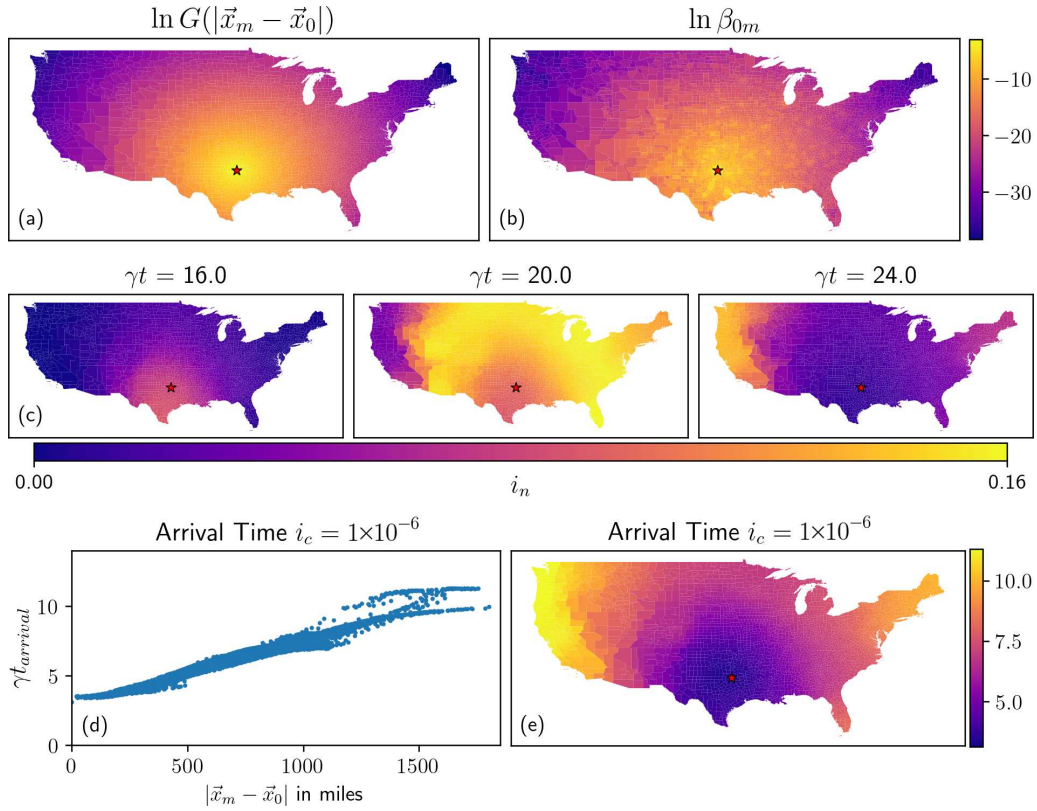
FIG. 13. [(a) and (b)] Commuting distribution and derived contact matrix elements measured with respect to Dallas, Texas (star), using the the commuting parameters obtained from Ref. [1]: $P_{nm} \sim N_m^\zeta e^{-|\vec{x}_n - \vec{x}_m|/l}$, $l = 51$ mi, $\zeta = 0.64$. (c) Infectious spread from Dallas, Texas, with $R_0 = 2$ and $I_0 = 1$. Three time snapshots of the infection fraction are shown. (d) Arrival time as a function of distance from Dallas and (e) displayed on the map.

infection quickly reaches the boundary (which could be the result of a long-tailed commuting distribution or an infection wave front whose size is comparable to the size of the domain), then the disease will be undetected for a characteristic offset time, but once it is detected at one location, it will soon be detected everywhere. The former case can be modeled using a system of reaction-diffusion equations and the latter using the spatially independent SIR model. In these two limits, the exact form of the commuting probabilities is unimportant. However, there is an intermediate regime where both the exact commuting distribution and the asymmetry in the commuting probability matter. In order to correctly capture this intermediate regime, we had to consider the commuting dynamics of both the susceptible and the infected individuals, leading to a contact matrix that is nonlinear in the commuting probability.

Although we have not focused on the spreading due to long-distance air travel, such dynamics could be incorporated into the commuting probabilities. However, on scales where the dynamics are dominated by commuters, the spatially embedded infectious spread considered in this paper will dominate. While the mathematical literature tends to focus on the limiting behavior far from the infection source, realistically, the infection may never achieve this limit on scales where the commuter dynamics dominate. For that reason, our paper has focused on both the short-term and long-term arrival time behavior. In particular, the offset time is defined for even a single county, so the techniques developed here can elucidate the infectious spread at scales as small as the

step size at which data are taken. The behavior close to the infection origin can be understood as a transition from an initial dispersal-dominated regime where the disease is spreading thin throughout counties near the origin to a growth-dominated regime where the infection at each location grows exponentially until it is detected. There is an interesting trade-off in the short-term and long-term behavior of an epidemic. In cases where people travel far, the disease can go undetected for a longer period of time and case counts will be everywhere low early on, but once the disease is detected at one location, it will be detected everywhere and the entire population will be experiencing the epidemic simultaneously. If, however, people remain close to home, then the disease will be detected sooner near the origin, but the infection will travel slower to neighboring counties, so the arrival time far from the origin is higher. In this way, the commuting patterns will dictate the times at which an infectious disease is detected at different locations when long-distance flights are neglected, but the total number of cases can only be lowered by reducing the number of contacts.

In characterizing the role of commuter distributions in disease spread, we made several simplifying assumptions that limit the predictive power of the commuter model. We assumed that the total number of contacts a person makes is independent of their home location and time, but one could easily relax this assumption. Our model is deterministic, so it neglects the possibility of finite-time extinction. We assumed zero latency period, lifetime immunity, and neglected births
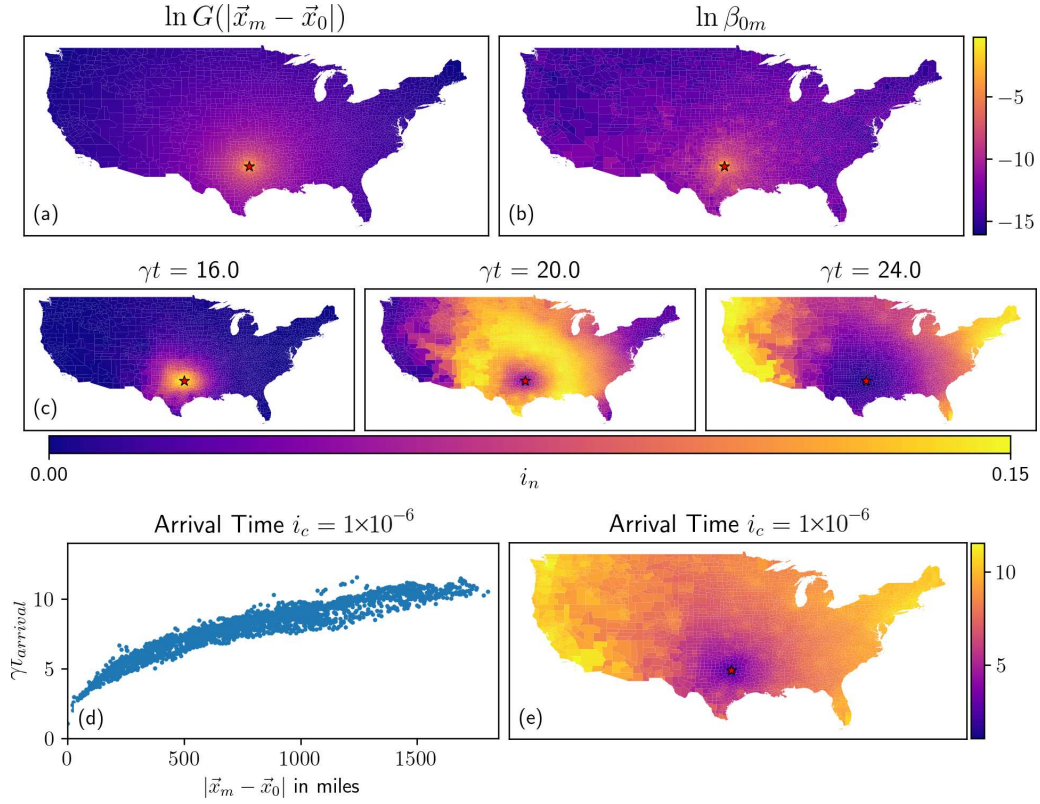
FIG. 14. [(a) and (b)] Commuting distribution and derived contact matrix elements measured with respect to Dallas, Texas (star), using the the commuting parameters obtained from Ref. [49]: $P_{nm} \sim N_m^\zeta (|\vec{x}_n - \vec{x}_m| + r_0)^{-p}$, $p = 3.05$, $\zeta = 0.64$. The small-scale cutoff (not considered in their paper) was chosen to be $r_0 = 10$ mi. (c) Infectious spread from Dallas, Texas, with $R_0 = 2$ and $I_0 = 1$. Three time snapshots of the infection fraction are shown. (d) Arrival time as a function of distance from Dallas and (e) displayed on the map.
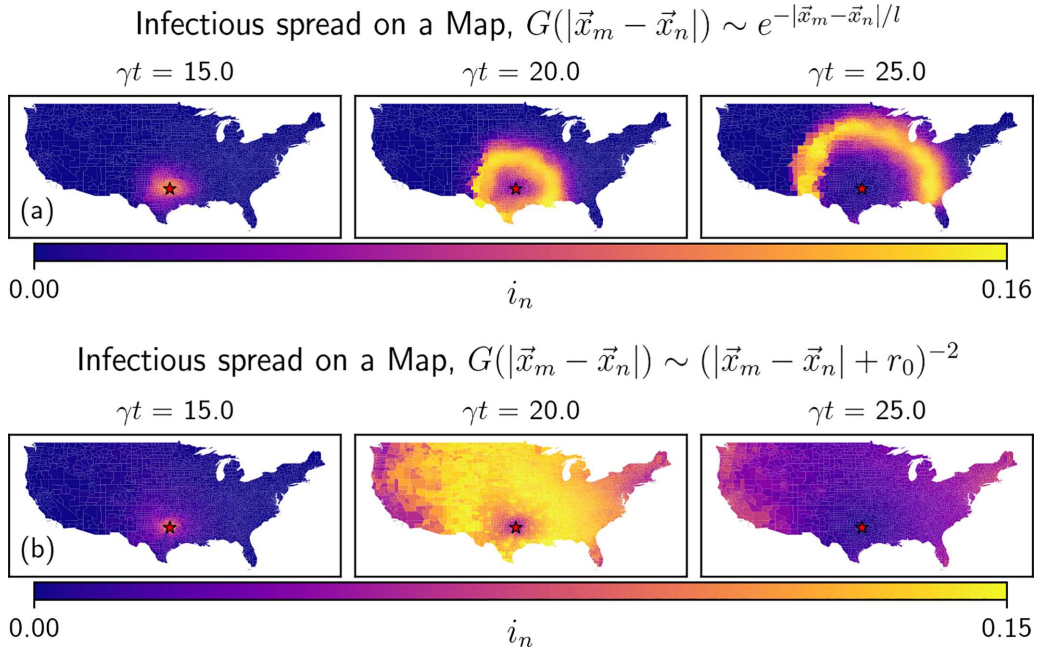

FIG. 15. (a) Infectious spread from Dallas, Texas (star), for a localized commuting distribution with $l = 15$ miles. (b) Infectious spread from Dallas, Texas, for a delocalized ($p = 2$) commuting distribution with $r_0 = 1$ mile. Additional parameters used for these simulations were $\zeta = 0$, $R_0 = 2$, and $I_0 = 1$. Three time snapshots of the infection fraction are shown for each case. The localized commuting distribution produces traveling waves from the infection source while the delocalized commuting distribution leads to nearly homogeneous infection growth across the country.

and deaths. The analysis presented here could be adapted to more complicated epidemic models or other social phenomena such as rumor spreading [51]. While the precise dynamics will depend on any new rate constants introduced, the lessons persist: Only localized commuting distributions give rise to local theories of dispersal, higher-order contact processes matter, and the early-time dynamics should not be ignored.

To summarize, we have demonstrated that commuter interactions give rise to complex disease-spreading phenomena. Our work relates the modern literature concerning metapopulations with the classical theories concerning continuous propagation of infection fronts. Traveling waves resulting from the interaction between mobile individuals capable of spreading disease have been previously studied, but the precise correspondence between a discrete Lagrangian metapopulation model and its reaction-diffusion counterpart has never been made. In particular, we highlighted the fact that the rate in the diffusion coefficient is precisely the infection growth rate since both arise from the same contact distribution. We also noted the possibility of a drift term; the infected population drifts toward higher population regions, but the infection fraction drifts toward lower population regions, so an individual in a small town is initially at a higher risk of getting sick than an individual in a big city. The arrival time has previously been used to characterize the spread of disease,

but our work defines and analyzes the offset time as a way to characterize the onset of an outbreak. Finally, this is the first time the role of key parameters that describe human mobility (l, r_0, p, and ζ) has been systematically studied, including the complex behavior that occurs for delocalized (but not well-mixed) commuting distributions.

APPENDIX A: DERIVATION OF THE REACTION-DIFFUSION EQUATION

Beginning with (26), we can derive the reaction-diffusion system (32) by performing a series of Taylor expansions. Crucially, this is only valid when (21) is satisfied, such that all of the moments of our commuting distribution converge. We first estimate the fraction of people currently located at $\vec{y}$ who are infected. Since $G(|\vec{z} - \vec{y}|)$ is exponentially localized near $\vec{z} = \vec{y}$, only the values of i near $\vec{z} = \vec{y}$ will matter, so we can Taylor expand $i(\vec{z})$ around $i(\vec{y})$, and do the same for $N(\vec{z})$,

$$
\begin{aligned}
\frac{\int d^d z \, P(\vec{z}, \vec{y}) N(\vec{z}) i(\vec{z}, t)}{\int d^d z \, P(\vec{z}, \vec{y}) N(\vec{z})} &\approx i(\vec{y}, t) + \frac{\int d^d z \, P(\vec{z}, \vec{y}) N(\vec{z}) (z^\mu - y^\mu)}{\int d^d z \, P(\vec{z}, \vec{y}) N(\vec{z})} \partial_\mu i(\vec{y}, t) \\
&\quad + \frac{1}{2} \frac{\int d^d z \, P(\vec{z}, \vec{y}) N(\vec{z}) (z^\mu - y^\mu)(z^\nu - y^\nu)}{\int d^d z \, P(\vec{z}, \vec{y}) N(\vec{z})} \partial_\mu \partial_\nu i(\vec{y}, t) \\
&\approx i(\vec{y}, t) + \int d^d z \, G(\vec{z}, \vec{y})[1 + (1 - \zeta)\partial_\nu \ln N(\vec{y})(z^\nu - y^\nu)](z^\mu - y^\mu)\partial_\mu i(\vec{y}, t) \\
&\quad + \frac{1}{2} \int d^d z \, G(\vec{z}, \vec{y})(z^\mu - y^\mu)(z^\nu - y^\nu)\partial_\mu \partial_\nu i(\vec{y}, t) \\
&= i(\vec{y}, t) + \frac{\langle y^2 \rangle}{d}(1 - \zeta)\boldsymbol{\nabla} \ln N(\vec{y}) \cdot \boldsymbol{\nabla} i(\vec{y}, t) + \frac{1}{2}\frac{\langle y^2 \rangle}{d}\nabla^2 i(\vec{y}, t).
\end{aligned}
\tag{A1}
$$

Using the same procedure, we can calculate the probability that a contact made by someone living at $\vec{x}$ is with an infected,

$$
\begin{aligned}
\int d^d y \, P(\vec{x}, \vec{y}) \frac{\int d^d z \, P(\vec{z}, \vec{y}) N(\vec{z}) i(\vec{z}, t)}{\int d^d z \, P(\vec{z}, \vec{y}) N(z)} &\approx \int d^d y \, P(\vec{x}, \vec{y})\left[i(\vec{y}, t) + \frac{\langle y^2 \rangle}{d}(1 - \zeta)\boldsymbol{\nabla} \ln N(\vec{y}) \cdot \boldsymbol{\nabla} i(\vec{y}, t) + \frac{1}{2}\frac{\langle y^2 \rangle}{d}\nabla^2 i(\vec{y}, t)\right] \\
&= \int d^d y \, G(\vec{x}, \vec{y})[1 + \zeta \partial_\nu \ln N(\vec{x})(y^\nu - x^\nu)] \\
&\quad \times \left[i(\vec{x}, t) + \partial_\mu i(\vec{x}, t)(y^\mu - x^\mu) + \frac{1}{2}\partial_\mu \partial_\nu i(\vec{x}, t)(y^\mu - x^\mu)(y^\nu - x^\nu)\right] \\
&\quad + \frac{\langle x^2 \rangle}{d}(1 - \zeta)\boldsymbol{\nabla} \ln N(\vec{x}) \cdot \boldsymbol{\nabla} i(\vec{x}, t) + \frac{1}{2}\frac{\langle x^2 \rangle}{d}\nabla^2 i(\vec{x}, t) \\
&= i(\vec{x}, t) + \frac{\langle x^2 \rangle}{d}\boldsymbol{\nabla} \ln N(\vec{x}) \cdot \boldsymbol{\nabla} i(\vec{x}, t) + \frac{\langle x^2 \rangle}{d}\nabla^2 i(\vec{x}, t).
\end{aligned}
\tag{A2}
$$

The same method was used to derive Eq. (60) where terms up to fourth order in derivatives were kept.

[1] D. Balcan, V. Colizza, B. Gonçalves, H. Hu, J. J. Ramasco, and A. Vespignani, Proc. Natl. Acad. Sci. USA **106**, 21484 (2009).

[2] L. Wang and X. Li, Chin. Sci. Bull. **59**, 3511 (2014).

[3] S. Riley, Science **316**, 1298 (2007).

[4] L. A. Rvachev and I. M. Longini, Math. Biosci. **75**, 3 (1985).

[5] D. Brockmann and D. D. Helbing, Science **342**, 1337 (2013).

[6] V. Colizza, A. Barrat, M. Barthélemy, and A. Vespignani, Proc. Natl. Acad. Sci. USA **103**, 2015 (2006).

[7] S. Charaudeau, K. Pakdaman, and P.-Y. Boëlle, PLoS One **9**, e83002 (2014).

[8] G. Le Treut, G. Huber, M. Kamb, K. Kawagoe, A. McGeever, J. Miller, R. Pnini, B. Veytsman, and D. Yllanes, Sci. Rep. **12**, 15946 (2022).

[9] J. S. Jia, X. Lu, Y. Yuan, G. Xu, J. Jia, and N. A. Christakis, Nature (London) **582**, 389 (2020).

[10] D. Calvetti, A. P. Hoover, J. Rose, and E. Somersalo, Mathematics **9**, 1861 (2021).

[11] M. Gatto, E. Bertuzzo, L. Mari, S. Miccoli, L. Carraro, R. Casagrandi, and A. Rinaldo, Proc. Natl. Acad. Sci. USA **117**, 10484 (2020).

[12] A. Gautreau, A. Barrat, and M. Barthélemy, J. Stat. Mech.: Theory Exp. (2007) L09001.

[13] F. Iannelli, A. Koher, D. Brockmann, P. Hövel, and I. M. Sokolov, Phys. Rev. E **95**, 012313 (2017).

[14] T. W. Russell, J. T. Wu, S. Clifford, W. J. Edmunds, A. J. Kucharski, and M. Jit, Lancet Publ. Health **6**, e12 (2021).

[15] D. Kendall, as discussed in M. Bartlett, J. R. Stat. Soc. A **120**, 64 (1957).

[16] D. Kendall, in *Mathematics and Computer Science in Biology and Medicine, Proceedings of Conference Held by Medical Research Council in association with the Health Departments, Oxford, July 1964* (Her Majesty's Stationery Office, London, 1965), pp. 213–225.

[17] D. Mollison, in *Proceedings of the Sixth Berkeley Symposium on Mathematical Statistics and Probability*, edited by L. Le Cam, J. Neyman, and E. Scott (University of California Press, Berkeley, Los Angeles, 1972), p. 579.

[18] L. Rass and J. Radcliffe, *Spatial Deterministic Epidemics*, Mathematical Surveys and Monographs (American Mathematical Society, Providence, RI, 2003).

[19] O. Diekmann, J. Math. Biol. **6**, 109 (1978).

[20] Y. Hosono and B. Ilyas, Math. Models Methods Appl. Sci. **05**, 935 (1995).

[21] M. Martcheva, *An Introduction to Mathematical Epidemiology*, Texts in Applied Mathematics, Vol. 61 (Springer US, New York, 2015).

[22] D. Brockmann, in *Reviews of Nonlinear Dynamics and Complexity*, Vol. 2, edited by H. G. Schuster (Wiley-VCH, Weinheim, 2009), pp. 1–24.

[23] W. O. Kermack and A. G. McKendrick, Proc. R. Soc. London, Ser. A **115**, 700 (1927).

[24] H. W. Hethcote, SIAM Rev. **42**, 599 (2000).

[25] R. A. Fisher, Ann. Eugen. **7**, 355 (1937).

[26] D. Mollison, Adv. Appl. Probab. **4**, 233 (1972).

[27] C. Cosner, J. Beier, R. Cantrell, D. Impoinvil, L. Kapitanski, M. Potts, A. Troyo, and S. Ruan, J. Theor. Biol. **258**, 550 (2009).

[28] Q. Yin, Z. Wang, C. Xia, M. Dehmer, F. Emmert-Streib, and Z. Jin, Appl. Math. Comput. **386**, 125517 (2020).

[29] A. Barrat, M. Barthélemy, R. Pastor-Satorras, and A. Vespignani, Proc. Natl. Acad. Sci. USA **101**, 3747 (2004).

[30] J. Arino and P. Driessche, in *Nonlinear Dynamics and Evolution Equations*, edited by H. Brunner, X. Zhao, and X. Zou (American Mathematical Society, Providence, 2006).

[31] V. Belik, T. Geisel, and D. Brockmann, Phys. Rev. X **1**, 011001 (2011).

[32] A. Lipshtat, R. Alimi, and Y. Ben-Horin, Sci. Rep. **11**, 15198 (2021).

[33] J. Arino and P. van den Driessche, Math. Popul. Stud. **10**, 175 (2003).

[34] W. Post, D. DeAngelis, and C. Travis, Math. Biosci. **63**, 289 (1983).

[35] H. Barbosa, M. Barthelemy, G. Ghoshal, C. R. James, M. Lenormand, T. Louail, R. Menezes, J. J. Ramasco, F. Simini, and M. Tomasini, Phys. Rep. **734**, 1 (2018).

[36] F. Simini, M. C. González, A. Maritan, and A.-L. Barabási, Nature (London) **484**, 96 (2012).

[37] R. Gallotti, A. Bazzani, S. Rambaldi, and M. Barthelemy, Nat. Commun. **7**, 12600 (2016).

[38] H. E. Daniels, J. Appl. Probab. **12**, 373 (1975).

[39] W. Wang, Y. Cai, M. Wu, K. Wang, and Z. Li, Nonlin. Anal. Real World Appl. **13**, 2240 (2012).

[40] U. Ebert and W. Van Saarloos, Physica D **146**, 1 (2000).

[41] P. B. Dieterle and A. Amir, Phys. Rev. E **104**, 014406 (2021).

[42] G. Birzu, O. Hallatschek, and K. S. Korolev, Proc. Natl. Acad. Sci. USA **115**, E3645 (2018).

[43] D. Aronson and H. Weinberger, Adv. Math. **30**, 33 (1978).

[44] D. del-Castillo-Negrete, B. A. Carreras, and V. E. Lynch, Phys. Rev. Lett. **91**, 018302 (2003).

[45] E. Hanert, E. Schumacher, and E. Deleersnijder, J. Theor. Biol. **279**, 9 (2011).

[46] O. Hallatschek and D. S. Fisher, Proc. Natl. Acad. Sci. USA **111**, E4911 (2014).

[47] US Census Bureau, https://www2.census.gov/programs-surveys/popest/datasets/2010-2019/counties/totals/.

[48] Plotly, https://raw.githubusercontent.com/plotly/datasets/master/geojson-counties-fips.json.

[49] C. Viboud, O. N. Bjørnstad, D. L. Smith, L. Simonsen, M. A. Miller, and B. T. Grenfell, Science **312**, 447 (2006).

[50] S. Chang, E. Pierson, P. W. Koh, J. Gerardin, B. Redbird, D. Grusky, and J. Leskovec, Nature (London) **589**, 82 (2021).

[51] C. Castellano, S. Fortunato, and V. Loreto, Rev. Mod. Phys. **81**, 591 (2009).